

XN-NF-78-34 (NP)

**GENERIC MECHANICAL AND THERMAL HYDRAULIC
DESIGN FOR EXXON NUCLEAR 14×14 RELOAD
FUEL ASSEMBLIES WITH ZIRCALOY GUIDE
TUBES FOR WESTINGHOUSE 2-LOOP
PRESSURIZED WATER REACTORS**

NOVEMBER 1978

RICHLAND, WA 99352

EXXON NUCLEAR COMPANY, Inc.

790126 0160

XN-NF-78-34 (NP)
ISSUE DATE: 01/12/79

GENERIC MECHANICAL AND THERMAL HYDRAULIC
DESIGN FOR EXXON NUCLEAR 14X14 RELOAD
FUEL ASSEMBLIES WITH ZIRCALOY GUIDE
TUBES FOR WESTINGHOUSE 2-LOOP
PRESSURIZED WATER REACTORS

Prepared by: Douglas J. Cook
D. J. Cook

Approved: J. F. Patterson
J. F. Patterson, Manager
Mechanical Engineering

Approved: G. A. Sofen
G. A. Sofen, Manager
Nuclear Fuels Engineering

Approved: D. C. Lehfeldt
D. C. Lehfeldt, Manager
Customer Projects

Accepted: W. S. Nechodom
W. S. Nechodom, Manager
Licensing and Compliance

EXXON NUCLEAR COMPANY, Inc.

NUCLEAR REGULATORY COMMISSION DISCLAIMER

IMPORTANT NOTICE REGARDING CONTENTS AND USE OF THIS DOCUMENT

PLEASE READ CAREFULLY

This technical report was derived through research and development programs sponsored by Exxon Nuclear Company, Inc. It is being submitted by Exxon Nuclear to the USNRC as part of a technical contribution to facilitate safety analyses by licensees of the USNRC which utilize Exxon Nuclear-fabricated reload fuel or other technical services provided by Exxon Nuclear for light water power reactors and it is true and correct to the best of Exxon Nuclear's knowledge, information, and belief. The information contained herein may be used by the USNRC in its review of this report, and by licensees or applicants before the USNRC which are customers of Exxon Nuclear in their demonstration of compliance with the USNRC's regulations.

Without derogating from the foregoing, neither Exxon Nuclear nor any person acting on its behalf:

- A. Makes any warranty, express or implied, with respect to the accuracy, completeness, or usefulness of the information contained in this document, or that the use of any information, apparatus, method, or process disclosed in this document will not infringe privately owned rights; or
- B. Assumes any liabilities with respect to the use of, or for damages resulting from the use of, any information, apparatus, method, or process disclosed in this document.

TABLE OF CONTENTS

	<u>Page</u>
1.0 INTRODUCTION AND SUMMARY	1
1.1 INTRODUCTION	1
1.2 SUMMARY.	1
2.0 FUEL ASSEMBLY DESCRIPTION	3
3.0 DESIGN CRITERIA	7
3.1 FUEL DESIGN CRITERIA SUMMARY	7
3.2 MECHANICAL DESIGN CRITERIA	8
3.3 MATERIAL PROPERTIES	10
3.3.1 Physical Properties of Zircaloy-4	10
3.3.2 Physical Properties of Fuel	14
4.0 FUEL ROD FAILURE MECHANISMS ANALYSIS.	31
4.1 CORROSION FAILURE.	32
4.2 MECHANICAL FAILURE MECHANISMS.	33
4.2.1 Strain Limiting Phenomena.	33
4.2.2 Pellet-Cladding Interaction.	34
4.2.3 Strain Limits.	35
4.2.4 Stress Limiting Phenomena.	36
4.2.5 Creep Collapse	37
4.3 MECHANICALLY ASSISTED FAILURE MECHANISM.	38

TABLE OF CONTENTS (Continued)

	<u>Page</u>
4.3.1 Stress Corrosion.	38
4.3.2 Fretting Corrosion.	39
5.0 COMPONENT MECHANICAL DESIGN ANALYSIS	42
5.1 FUEL RODS	42
5.1.1 General Description	42
5.1.2 Design Criteria	43
5.1.3 Cladding Strain Analysis.	44
5.1.4 Fuel Rod End Cap Analysis	49
5.1.5 Cladding Collapse	50
5.1.6 Cladding Strain Analysis	53
5.1.7 Pellet Design	56
5.1.8 Fuel Rod Bow Analysis	58
5.2 TIE PLATES.	61
5.2.1 General Description	61
5.2.2 Design Criteria	62
5.2.3 Holddown Spring Analysis.	63
5.3 GUIDE TUBE.	64
5.3.1 General Description	64
5.3.2 Design Criteria	65
5.3.3 Mechanical Design Analysis.	65
5.3.4 Hydraulic Design Analysis	70

TABLE OF CONTENTS (Continued)

	<u>Page</u>
5.4 GRID SPACERS	72
5.4.1 General Description.	72
5.4.2 Design Criteria.	73
5.4.3 Spring Characteristics	75
5.4.4 Structural Integrity	81
5.5 FUEL ASSEMBLY OVERALL STRUCTURE.	82
5.5.1 General Description.	82
5.5.2 Design Criteria.	83
5.5.3 Design Analysis.	84
6.0 FUEL TEMPERATURE ANALYSIS	103
7.0 REFERENCES.	107

LIST OF TABLES

<u>Table No.</u>		<u>Page</u>
2.1	Fuel Assembly and Component Description.	6
3.1	Material Strength Summary.	22
5.1	Steady State Stress Design Limits.	86
5.2	Summary Limiting Stress Intensity Conditions	87
5.3	Fuel History - Design Basis for Fuel Rod Prepressurization and Cladding Collapse and Strain Calculations.	88
5.4	Duty Cycles.	89
5.5	Cyclic Stress Summary.	90

LIST OF FIGURES

<u>Figure No.</u>		<u>Page</u>
3-1	Mechanical Strength of ENC Zircaloy-4 Tubing versus Temperature.	23
3-2	Ductility of ENC Zircaloy-4 Tubing versus Temperature. . . .	24
3-3	Review of Data Pertaining to the Effect of Fast Neutrons on the Change in Yield Stress in Zircaloy-4	25
3-4	Effect of Fast Neutron Irradiation at 500°F (260°C) on the Mechanical Properties of Zircaloy-2.	26
3-5	Effect of Temperature on Secondary Creep Rate of Zircaloy. .	27
3-6	Calculated Creep Rate versus Measured Creep Rate (In-Reactor Zircaloy Pressurized Tubes and Tensile Creep Specimens). . .	28
3-7	UO ₂ Thermal Conductivity as a Function of Temperature. . . .	29
3-8	Gap Closure of As-Fabricated Gap versus Irradiation Time . .	30
4-1	Axial Irradiation Growth of Zircaloy Tubing.	40
4-2	Cyclic Fatigue Design Curve for Irradiated Zircaloy-2 or -4 Room Temperature to 600°F (316°C). Total Irradiation Exposure 5.5×10^{21} nvt Fast Fluence (>0.625 eV)	41
5-1	Influence of Pellet Length on Rod Elongation	91
5-2	Effect of Pellet Geometry on Axial and Diametral Expansions	92
5-3	Comparison of Rod-To-Rod Spacing for All Data.	93
5-4	Comparison of Rod-To-Guide Tube Spacing for All Data	94
5-5	Fractional Channel Closure at Span as a Function of Assembly Average Exposure.	95
5-6	Affect of Spacer Cell Geometry on Axial Restraint.	96
5-7	Estimated Stress Relaxation vs. Fluence.	97

LIST OF FIGURES (Continued)

<u>Figure No.</u>		<u>Page</u>
5-8	Spacer Spring Deflection vs. Load Curves.	98
5-9	Illustration of Flow Induced Vibration of a Fuel Rod. . . .	99
5-10	Illustration of Forces and Deflections of Bowed Fuel Rod. .	100
5-11	Schematic Diagram of Fuel Bundle Striking the Top of a Spacer Grid During Bundle Insertion Into Core	101
5-12	Test Arrangement.	102

GENERIC MECHANICAL AND THERMAL HYDRAULIC
DESIGN FOR EXXON NUCLEAR 14X14 RELOAD
FUEL ASSEMBLIES WITH ZIRCALOY GUIDE
TUBES FOR WESTINGHOUSE 2-LOOP
PRESSURIZED WATER REACTORS

1.0 INTRODUCTION AND SUMMARY

1.1 INTRODUCTION

The purpose of this document is to provide a generic summary of the design criteria, technical bases, analyses, and test results related to the design of Exxon Nuclear (ENC) 14x14 reload fuel assemblies with zircaloy guide tubes for Westinghouse 2-loop PWR's. The format of this report is in conformance with the NRC Standard Review Plan for the Fuel System Design. The Exxon Nuclear fuel assemblies are designed to be compatible with fuel assemblies in the reactor and to comply with regulatory requirements.

1.2 SUMMARY

The ENC fuel assembly design is a 14x14 array with 179 fuel rods, 16 guide tubes, and one (1) instrumentation tube. The ENC fuel design is similar to the Westinghouse fuel design with several important differences. The ENC etched fuel rod design has 30 mil wall thickness Zircaloy-4 cladding, which is approximately 23% thicker than the Westinghouse cladding, and the fuel rod design has mil wall thickness cladding. For standard

fuel rod assemblies, the fuel pellets are short and dished with a mean fuel density of theoretical. For gadolinia burnable poison rod assemblies, if part of the fuel assembly design, the fuel pellets are the same configuration as the standard UO_2 pellet with Gd_2O_3 dispersed in a UO_2 matrix. The bi-metallic spacers are a Zircaloy-4 structure with Inconel springs. The fuel assembly upper tie plate is mechanically locked to the Zircaloy-4 guide tubes to allow inspection of irradiated fuel rods and the capability to replace a fuel rod.

This generic document is divided into seven sections.

Section 2.0 describes the ENC 14x14 fuel assembly.

Section 3.0 summarizes the design criteria and technical bases for the fuel performance analysis and includes material properties and property behavior models and cladding stress, strain, and collapse requirements.

Section 4.0 discusses corrosion, corrosion-mechanical, and mechanical fuel failure mechanisms.

Section 5.0 contains the mechanical analysis for individual components and the total fuel assembly.

Section 6.0 summarizes the fuel thermal analysis.

Section 7.0 is references.

2.0 FUEL ASSEMBLY DESCRIPTION

The ENC 14x14 reload fuel assembly design with zircaloy guide tubes for Westinghouse 2-loop reactors is a 14x14 square array with 179 fuel rods, 16 control rod guide tubes, and one (1) instrumentation tube.

The fuel rod cladding is Zircaloy-4 cold worked and lightly stress relieved. Each standard fuel rod contains a 144.0 inches long column of fuel pellets pressed and sintered to theoretical density. The pellets are dished on both ends

Gadolinia

poison rod assemblies, if part of the fuel assembly design, contain fuel pellets the same configuration as the standard UO_2 pellet with Gd_2O_3 dispersed in a UO_2 matrix. The pellet column has an alumina (Al_2O_3) disc at each end to lower the temperature of the fission gas and reduce the transient thermal gradients in the lower end cap.

The fuel rod upper plenum contains an Inconel compression spring to prevent fuel column separation during fabrication and shipping. The upper end cap is a Zircaloy-4 plug-type end cap with design features to allow remote under water fuel rod handling. The lower end cap is a Zircaloy-4 plug-type end cap with a truncated cone exterior to aid fuel rod reinsertion into the fuel assembly during inspection and/or reconstruction in the reactor fuel storage pool. Both end caps are seal welded to the cladding during fuel rod assembly. Fuel rod identification is maintained by a

stamped serial number on the lower end cap conical surface. Fuel rods are pressurized with helium, which provides a good heat transfer medium, to insure freestanding cladding throughout the design life.

Fuel rod pitch is maintained by seven (7) bi-metallic spacers. The spacers are a welded Zircaloy-4 structure with Inconel 718 springs and are resistance spot welded to the guide tubes. The spacers are axially positioned so that the thermal hydraulics will be compatible with existing fuel assemblies. Each guide tube has a reduced diameter on the lower end to provide dashpot damping for the control rods. The guide tubes are mechanically attached to the upper and lower tie plates.

The upper tie plate assembly is a machined stainless steel casting which has four (4) Inconel holddown spring assemblies. These springs are attached to the tie plate by clamps and cap screws. The lower tie plate assembly is a machined stainless steel casting. The spacers, guide tubes, and tie plates form the structural framework of the fuel assembly.

The fuel rods are axially positioned with the upper and lower end caps approximately equidistant from the upper and lower tie plates. Axial fuel rod growth (of the active fuel length) is allowed for by the clearance between the fuel rod end caps and tie plates. The upper tie plate assembly can be mechanically removed and reinstalled on a fuel assembly (under water in a fuel pool) to allow inspection of irradiated fuel rods and the capability to replace a fuel rod.

A fuel assembly and its components are described in Table 2.1.

Table 2.1 Fuel Assembly and Component Description

<u>Component</u>	<u>Material</u>	<u>Design Characteristics</u>
Fuel Assembly ENC Drawing	--	Array - 14x14 Assembly Pitch - 7.803 in. Rod Pitch - 0.556 in. Length - 159.7 in. Distance between tie plates - 153.6 in. 179 Fuel Rods, 16 Guide Tubes, 1 Instrumentation Tube, 7 spacers (6 Within Active Fuel Zone)
Fuel Rod Assembly ENC Drawing	--	Total Length - 152.065 in. Active Fuel Length - 144.00 in.
Fuel Pellet		
Cladding		
Plenum Spring		
Spacers		
Guide Tube		
Guide Tube Assembly		

3.0 DESIGN CRITERIA

3.1 FUEL DESIGN CRITERIA SUMMARY

- 3.1.1 The fuel assemblies shall be mechanically compatible with the reactor core, steam supply system, fuel handling tools and system, existing fuel, control rods (full and part length), burnable poison, and thimble plugging devices.
- 3.1.2 The EWC fuel shall be compatible with the existing fuel assemblies on the basis of coolant flow and neutronic characteristics.
- 3.1.3 The fuel shall be designed to achieve a minimum departure from Nucleate Boiling Ratio of ≥ 1.3 at design overpower conditions using the W-3 correlation (or an equivalent) plus correction factors which have been accepted by NRC for the purpose of licensing the fuel design described herein.
- 3.1.4 The design shall incorporate a 14 x 14 square fuel rod array.
- 3.1.5 The fuel assemblies shall be designed to minimize the peak cladding temperature following a postulated loss of coolant accident (LOCA) consistent with current licensing criteria.

3.1.6 Reactor Conditions for Design Analysis

The reactor conditions assumed for mechanical design analyses were compiled from data on individual Westinghouse reactors with 14x14 fuel assemblies and were selected to produce the most conservative design.

Rated Heat Output	1520-1650 MWt
Nominal System Pressure	2250 psia
Total Coolant Flow Rate	$67.3-68.2 \times 10^6$ lbs/hr
Effective Coolant Flow Rate	$61.3-65.2 \times 10^6$ lbs/hr
Average Flow Velocity, ft/sec	14.8
Nominal Inlet Temperature	530.0-545.3°F
Total Plenum to Plenum Fuel Assembly Pressure Drop	24.8 psi at core Avg. velocity of ft/sec.
No. of Assemblies in Core	121

3.2 MECHANICAL DESIGN CRITERIA

3.2.1 Fuel Rod Design Criteria

a)

b)

c)

d)

3.2.2 Tie Plate Design Criteria

- a) The strength of the upper and lower tie plates shall be sufficient to withstand reactor holddown forces, hydraulic forces, differential thermal expansion forces, and handling and transport forces. The dynamic loads for vertical handling shall be assumed to be equal to times the dry assembly weight.
- b) The holddown springs must provide a nominal holddown load on a fuel assembly to prevent levitation under normal reactor operation conditions. The springs shall have an operating length range to accommodate differential thermal expansion and still maintain sufficient holddown forces.

3.2.3 Guide Tube Design Criteria

With the guide tubes, spacers, and tie plates assembled into a framework, the guide tubes and attachment hardware shall provide, throughout the design life of the fuel assembly, adequate strength to support the weight of the fuel assembly, support the holddown forces, resist forces from fuel rod-guide tube differential thermal expansion, and provide channels for control rod insertion.

3.2.4 Grid Spacer Design Criteria

- a) Spring and structural component materials shall retain adequate strength under operating conditions to ensure functional operation throughout the design life of the fuel.
- b) The minimum spring force shall be sufficient to restrain fuel rod thermal and mechanical bow, minimize flow induced vibrations, and prevent fatigue corrosion at spacer-fuel rod contact points. Irradiation induced stress relaxation shall be considered in establishing the minimum spring force.
- c)

3.2.5 Thermal Design Criteria

- a) The maximum fuel temperature (at overpower) shall not exceed the fuel melting temperature.
- b)

3.3 MATERIAL PROPERTIES

The material strength properties of major components are summarized in Table 3.1.

3.3.1 Physical Properties of Zircaloy-4

a) Thermal Conductivity

Thermal conductivity for Zircaloy-4 is based on data published by . The relationship is as follows:

$$K =$$

where:

$$T = \text{temperature, } F^{\circ}$$

b) Thermal Expansion

Thermal expansion used for Zircaloy-4 is as established by

c) Elastic Modulus and Poisson's Ratio

The temperature dependence of the modulus of elasticity, E , is based on as follows:

$$E \text{ (psi)} =$$

Poisson's ratio for design calculations is as follows:

Room Temperature , $\mu =$

Elevated temperature, $\mu =$

d) Effect of Temperature on Strength and Ductility

The effect of temperature on longitudinal ultimate and yield stress for Zircaloy-4 cladding is shown in Figure 3-1.⁽³⁾ Based upon ENC test data, the minimum yield strength as a function of temperature over the range of interest for fuel rods is described by the following equation:

$$\sigma_{\text{yield}} =$$

where:

T = temperature in °F

For design calculations, transverse strength is considered equivalent to longitudinal strength. However, the transverse strength in a biaxial stress condition, such as an internally pressurized fuel rod, is greater than longitudinal strength by 35%, assuming isotropic behavior, and about 55% for anisotropic behavior. Hill⁽⁴⁾ and Backofen, et al.,⁽⁵⁾ have shown that the plane stress yield condition for an anisotropic material can be represented by:

$$\sigma_y^2 \left(\frac{R(P+1)}{P(R+1)} + \alpha^2 - 2\alpha \frac{R}{R+1} \right) = X^2$$

where:

X = longitudinal yield strength

σ_y = transverse (circumferential) yield stress for subject stress ratio

R is defined as the ratio of the contractile strain in the radial direction to the contractile strain in the circumferential direction as determined in an uniaxial longitudinal tensile test. For isotropic material, R is equal to 1.0, and the percent of wall thinning is the same as the percent of diameter reduction. For a hexagonal lattice material such as zircaloy with only one slip system, isotropic behavior in tubing occurs only when the basal poles are oriented 45° to the radial direction.

Ductility (total axial elongation) of ENC tubing as a function of temperature is shown along with data from Reference 3 in Figure 3-2.

e) Effects of Irradiation on Strength and Ductility

Fuel rod cladding is strengthened and hardened by irradiation (except at temperatures where in-situ annealing occurs) as illustrated in Figure 3-3⁽⁶⁾. Increased strength due to irradiation hardening is not included in fuel rod design. The strength of the cladding at beginning-of-life (BOL) is assumed to be constant throughout the design lifetime.

Irradiation effects reduce the ductility of the cladding as shown in Figure 3-4⁽⁷⁾. When the fast fluence exceeds n/cm^2 , at high strain rates the total elongation approaches a and uniform elongation At slow strain rates (such as in creep tests) uniform elongation is

f) Creep Rate Characteristics

Zircaloy creep rate for fuel rod design is based on a general relationship developed by

$$\dot{\epsilon} =$$

At temperatures below 350°C (662°F), data result in the following equation for creep rate:

$$\dot{\epsilon} =$$

where:

At temperatures above 350°C (622°F), data from results in the following equation for creep rate:

$$\dot{\epsilon} =$$

where:

Figure 3-5 compares the two equations for creep analysis. Figure 3-6 compares the calculated strain rates with measured strain rates. (8,9,10,11,12)

g) Plasticity

For all analyses, the steady state plastic deformation is assumed to be a creep mechanism described by the equations above. These creep relationships are discussed in the RODEX manual⁽¹³⁾.

3.3.2 Physical Properties of Fuel

a) Thermal Expansion

The thermal expansion model for UO_2 is based on relationship:

$$\frac{\Delta L}{L} =$$

where:

T = temperature, °C

The curve provides a conservative design limitation over the entire UO_2 temperature spectrum as compared to the data of

b) Thermal Conductivity

The thermal conductivity function for UO_2 is from data:

$$K(T) =$$

where:

T = temperature, $^{\circ}C$

$K(T)$ = thermal conductivity of UO_2 , watts/cm $^{\circ}C$.

This equation applies to UO_2 ; the curve of conductivity versus temperature is shown in Figure 3-7.

Since this conductivity curve is only applicable for fuel, a density (porosity) correction factor is applied for fuel with densities other than with the following expression :

c) Melting Point

The value for the UO_2 melting point (unirradiated) is 2805 $^{\circ}C$ (5081 $^{\circ}F$). Based on measurements by (18)

the melting point is

$$T_m =$$

where:

T_m = melting point, °C

d) Swelling

The fuel swelling model is based on the empirical model of Geithoff, et al., (19) which incorporates the following effects:

- In the lower temperature fuel regions, small bubbles form and redissolve. The low swelling rates are largely dependent upon the solid fission product contribution.
- In the higher temperature fuel regions where fuel restructuring occurs, bubbles can migrate to grain boundaries and coalesce to produce a higher swelling rate until the grain boundary bubbles finally interconnect to form passages to open porosity and cracked interfaces. (The exposures where gross interconnection occurs in LMFBR fuel rods, for which the model was developed, are greater than those experienced in the LWR fuel rods.)

- In high temperature regions where columnar grains are formed, bubbles rapidly migrate, and the inert fission gases are released to open surfaces. The net swelling in these regions is smaller than in the equiaxed restructured regions and is largely dependent upon the solid fission products. Most LWR fuel rods have only a small portion of the fuel volume in these high temperature regions; hence, fission gas release is the primary mechanism associated with these fuel regions.

The swelling relations are as follows:

$$\Delta V/V =$$

$$T =$$

where:

$$\Delta V/V = \text{swelling per unit volume, (in}^3/\text{in}^3)$$

$$T = \text{average fuel region temperature (}^\circ\text{F)}$$

$$BU = \text{fuel region burnup (MWD/MTU)}$$

From the preceding relationships, between 2372°F (1300°C) and 3092°F (1700°C) dish volume is decreased only by the fuel in the dish regions. The incubation period in which non-densified porosity is filled by swelling is determined by the relationship:

$$BU_I =$$

$$BU_I = \text{incubation period with no swelling (MWD/MTU)}$$

$$I = \text{fraction of theoretical density before densification}$$

For the reference after densification design of 0.965 which is in the AEC report on densification⁽²⁰⁾, the resultant incubation period corresponds to a burnup of 6,800 MWD/MTU.

e) Densification

Densification of a UO_2 fuel pellet can result in decreased fuel pellet volume and increased clearance in the cladding gap. AEC evaluation of available data led to a model⁽²⁰⁾ to calculate the effect of densification data on radial gaps. The model is:

$$\Delta g_{\max} = \left[\frac{0.965 - \rho_i + 2\sigma}{3} \right] r_{ps}$$

where:

Δg_{\max} = radial gap increase

r_{ps} = nominal as-fabricated pellet radius

ρ_i = nominal as-fabricated density, fraction of theoretical

σ = standard deviation of the fabricated density

A 2σ limit on pellet density maximizes the calculated radial shrinkage and yields conservatively low gap coefficients. The 2σ limit results in a higher level of initial stored energy in the fuel than the case where radial shrinkage of the fuel is not considered. Although the maximum magnitude of possible radial shrinkage for the gap coefficient evaluation has been identified, the kinetics of this phenomenon have not been fully established.

Examination of density changes in irradiated fuel have reportedly shown that no temperature-independent densification occurs for exposure times of less than 14 hours of power operation, but that after 2000 hours of reactor operation fuel densification has probably been completed⁽²⁰⁾. This time frame for fuel densification is also supported by observations of in-core neutron flux distribution measurements which indicated local power spikes only after several hundred hours (300 to 400 reactor full power hours) of reactor operation⁽²¹⁾.

Furthermore, it has been shown qualitatively that a diffusion-controlled process of pore annihilation provides densification times that are consistent with the in-reactor neutron flux distribution measurements. Therefore, a time-dependent model for the fuel densification has been included in the ENC RODEX⁽¹³⁾ program. The model assumes the fuel densifies to within hours of start of reactor operation.

The expressions for the density increase which results from densification are a function of initial pellet density and irradiation time. For initial densities of 92.0% and higher, the following expressions are applicable:

$$\Delta\rho/\Delta\rho_{\max} =$$

$$\Delta\rho/\Delta\rho_{\max} =$$

$$\Delta\rho/\Delta\rho_{\max} =$$

where:

$$\Delta\rho/\Delta\rho_{\max} = \frac{t}{t_{\max}} \rho_i$$

ρ_i = nominal as-fabricated pellet density.

In the above expressions, t is effective full power hours (EFPH). These densification rate expressions were developed from the experimental data of Hanevik, et al. (22)

f) Cracking (Pellet Relocation)

It is clear from experimental observations that an oxide fuel pellet will experience thermal stresses sufficient to cause significant cracking. (23,24) The most noticeable physical result of cracking is an increase in the radial dimensions of the fuel pellet. A detailed investigation of approximately 80 irradiated fuel pellet cross-sections has shown that pellet cracking results in substantial closure of the pellet-to-cladding gap (25). This conclusion was based on observation of fuel with a broad range of physical parameters irradiated in nine reactors. These fuels exhibited a mean closure of 65% of the as-fabricated gap at room temperature after about 600 hours of irradiation (the first two or three power cycles).

Because the gap closure measurements reported in Reference 25 were based on the as-fabricated gap at room temperature, the radial dimensional change in the fuel pellet due to cracking is evaluated on the basis of cold pellet-to-cladding clearance as follows:

Although the fuel pellet radius change which results from pellet cracking is calculated on the basis of irradiation time, it is important to recognize that the effects of all variables which might affect gap closure, whether identified or not, are included in the basic data which developed the correlation; i.e., power cycling, crack healing, densification and cladding restraint. Figure 3-8 shows an average fit of the gap closure data and the cracking curve from which the gap closure (pellet relocation) was calculated.

TABLE 3.1
MATERIAL STRENGTH SUMMARY

<u>Item</u>	<u>Material</u>	<u>Minimum Tensile Strength Requirements</u>			
		<u>Room Temperature</u>		<u>Elevated Temperature</u>	
		<u>Ultimate (psi)</u>	<u>Yield (psi)</u>	<u>Ultimate (psi)</u>	<u>Yield (psi)</u>
Cladding	Zircaloy-4				
End Caps	Zircaloy-4				
Tie Plate Castings	304L SS				
Guide Tube	Zircaloy-4				
Guide Tube Lower Sleeve	Zircaloy-4				
Guide Tube Upper Sleeve	Zircaloy-4				
Guide Tube Cap Screw	304L SS				
Guide Tube Locking Ring and Lug	Inconel X-750				
Spacer Grid	Zircaloy-4				
Spacer Springs	Inconel 718				
Holddown Springs	Inconel 718				
Coil Springs	Inconel X-750				

23

XN-NF-78-34 (NP)

Temperature, °C

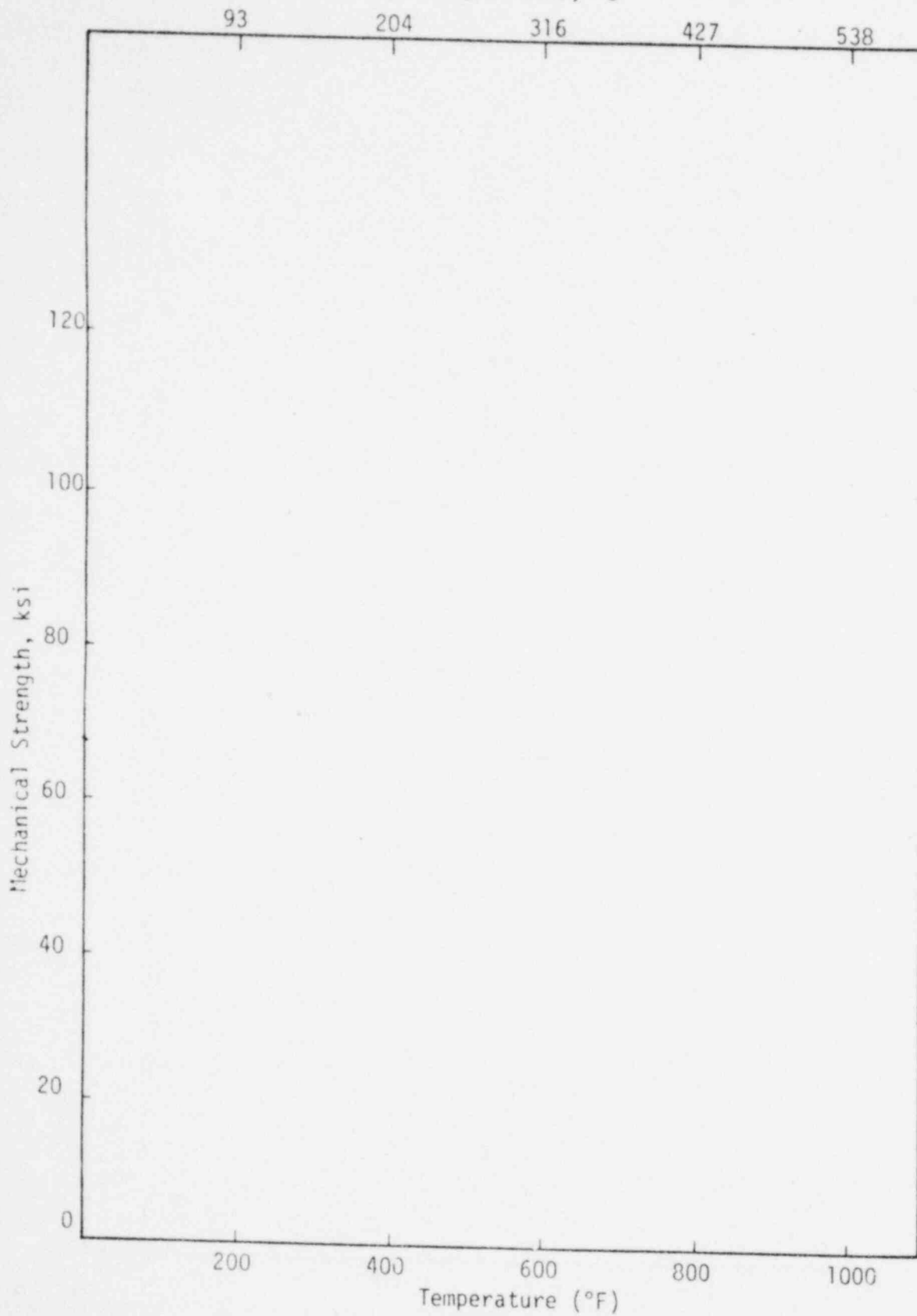


FIGURE 3-1 MECHANICAL STRENGTH OF ENC ZIRCALOY-4 TUBING VERSUS TEMPERATURE

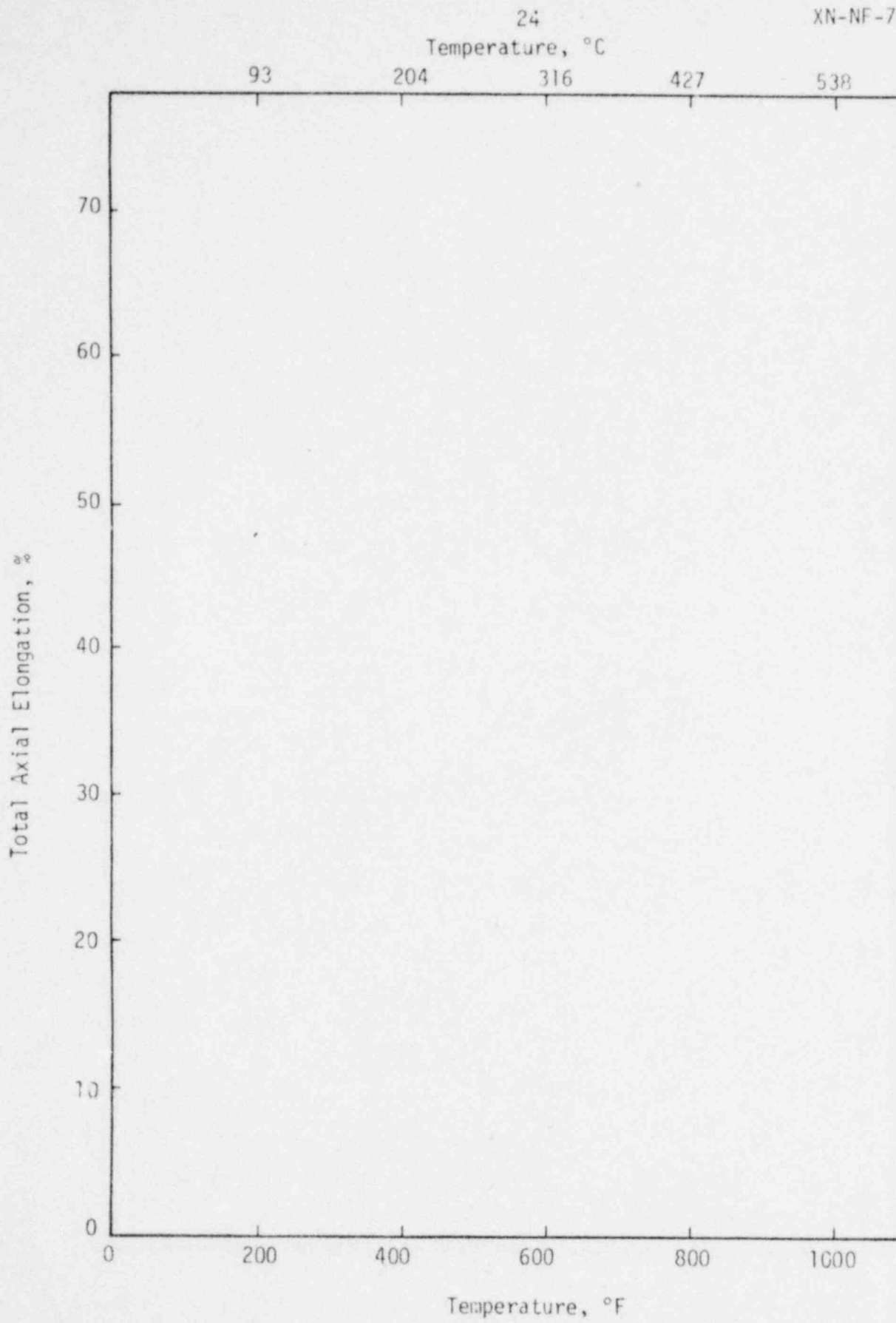


FIGURE 3-2

DUCTILITY OF ENCL ZIRCALOY-4
TUBING VERSUS TEMPERATURE

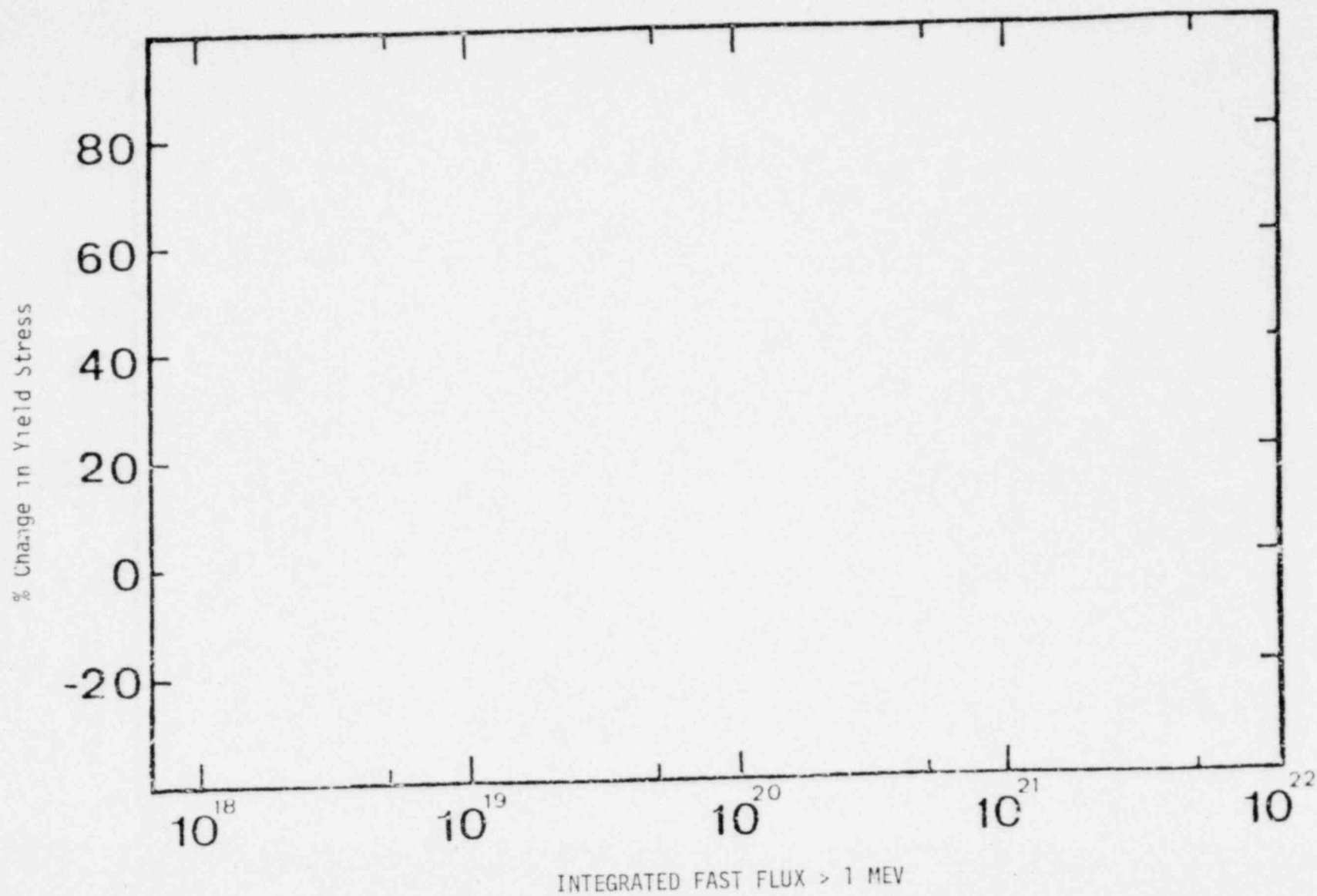


FIGURE 3-3 REVIEW OF DATA PERTAINING TO THE EFFECT OF FAST NEUTRONS ON THE CHANGE IN YIELD STRESS IN ZIRCALOY-4 (Reference 6)

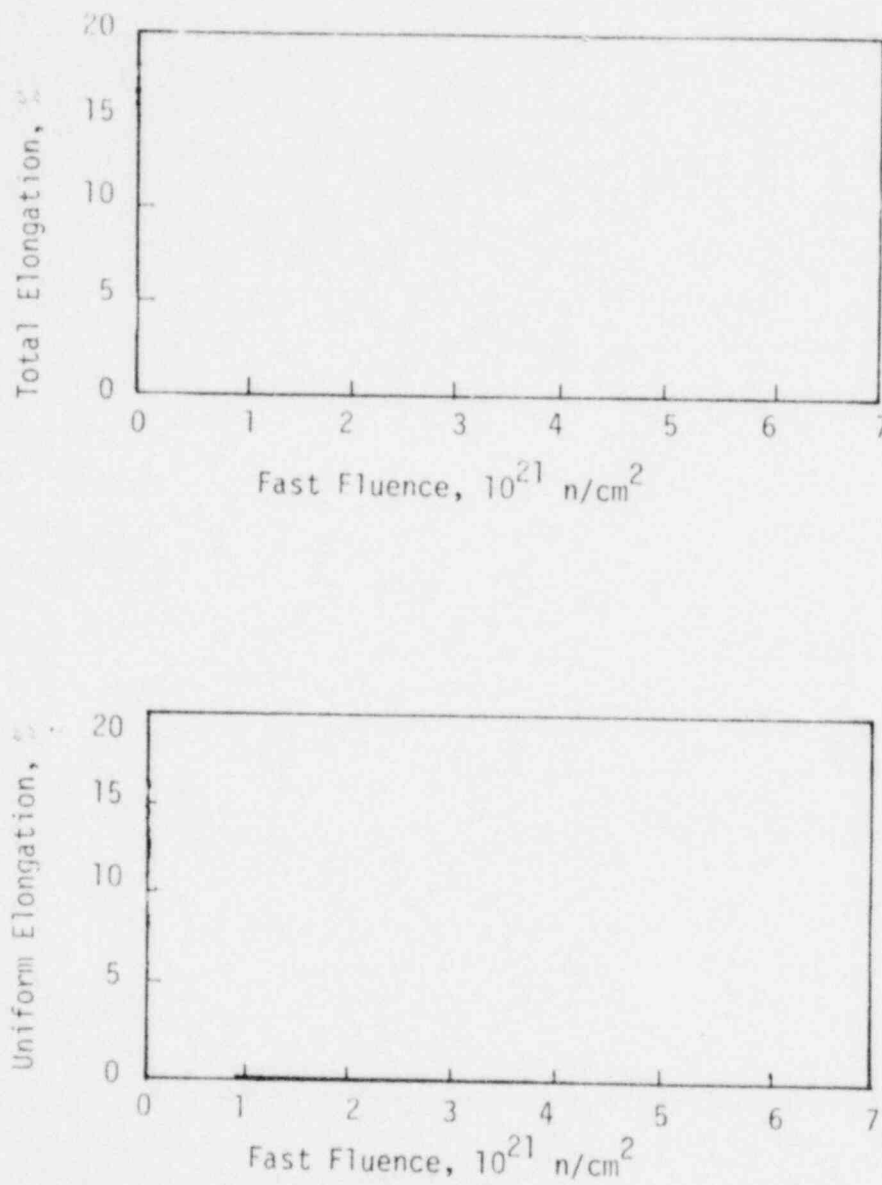


FIGURE 3-4 EFFECT OF FAST NEUTRON IRRADIATION AT 500°F (260°C) ON THE MECHANICAL PROPERTIES OF ZIRCALOY-2 (Reference 7)

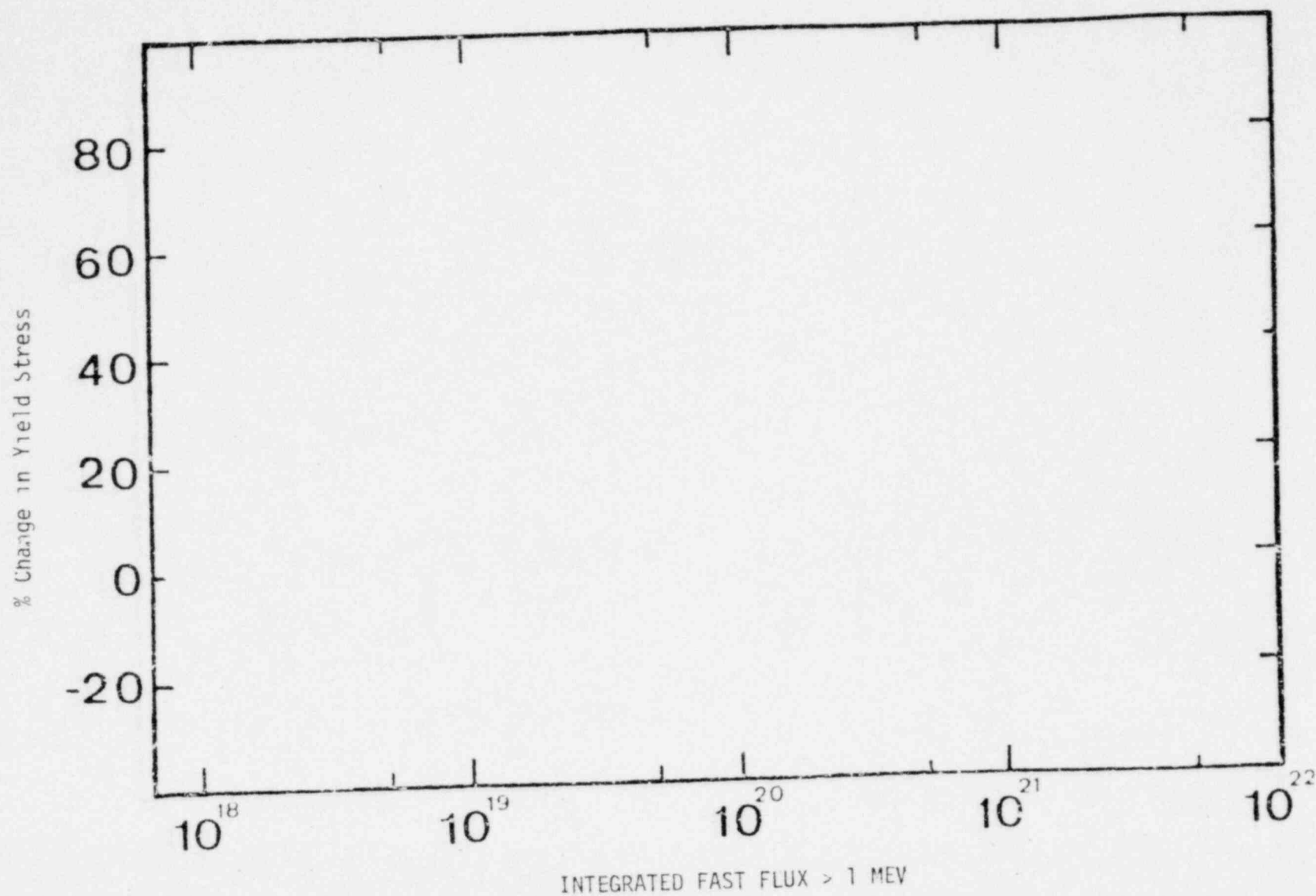


FIGURE 3-3 REVIEW OF DATA PERTAINING TO THE EFFECT OF FAST NEUTRONS ON THE CHANGE IN YIELD STRESS IN ZIRCALOY-4 (Reference 6)

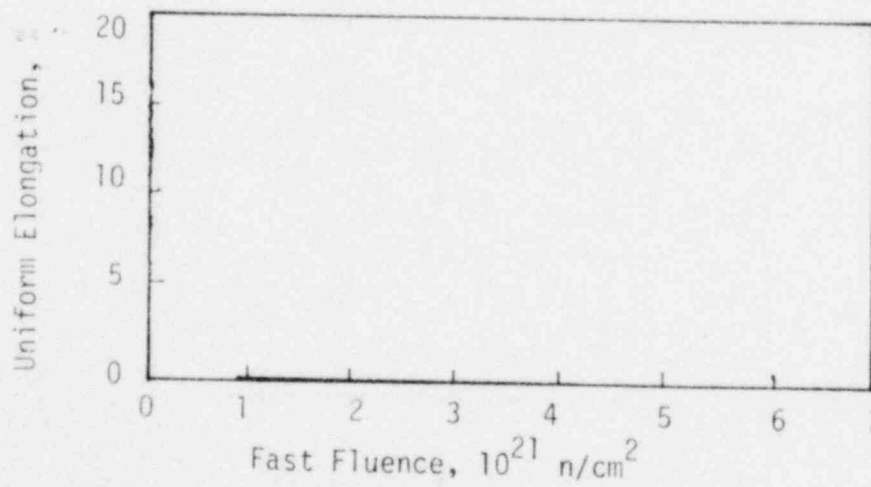
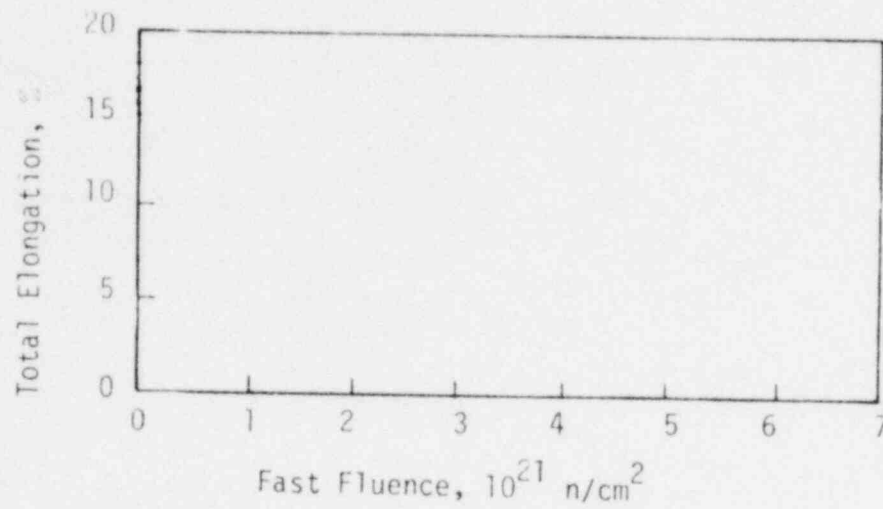


FIGURE 3-4 EFFECT OF FAST NEUTRON IRRADIATION
AT 500°F (260°C) ON THE MECHANICAL
PROPERTIES OF ZIRCALOY-2 (Reference 7)

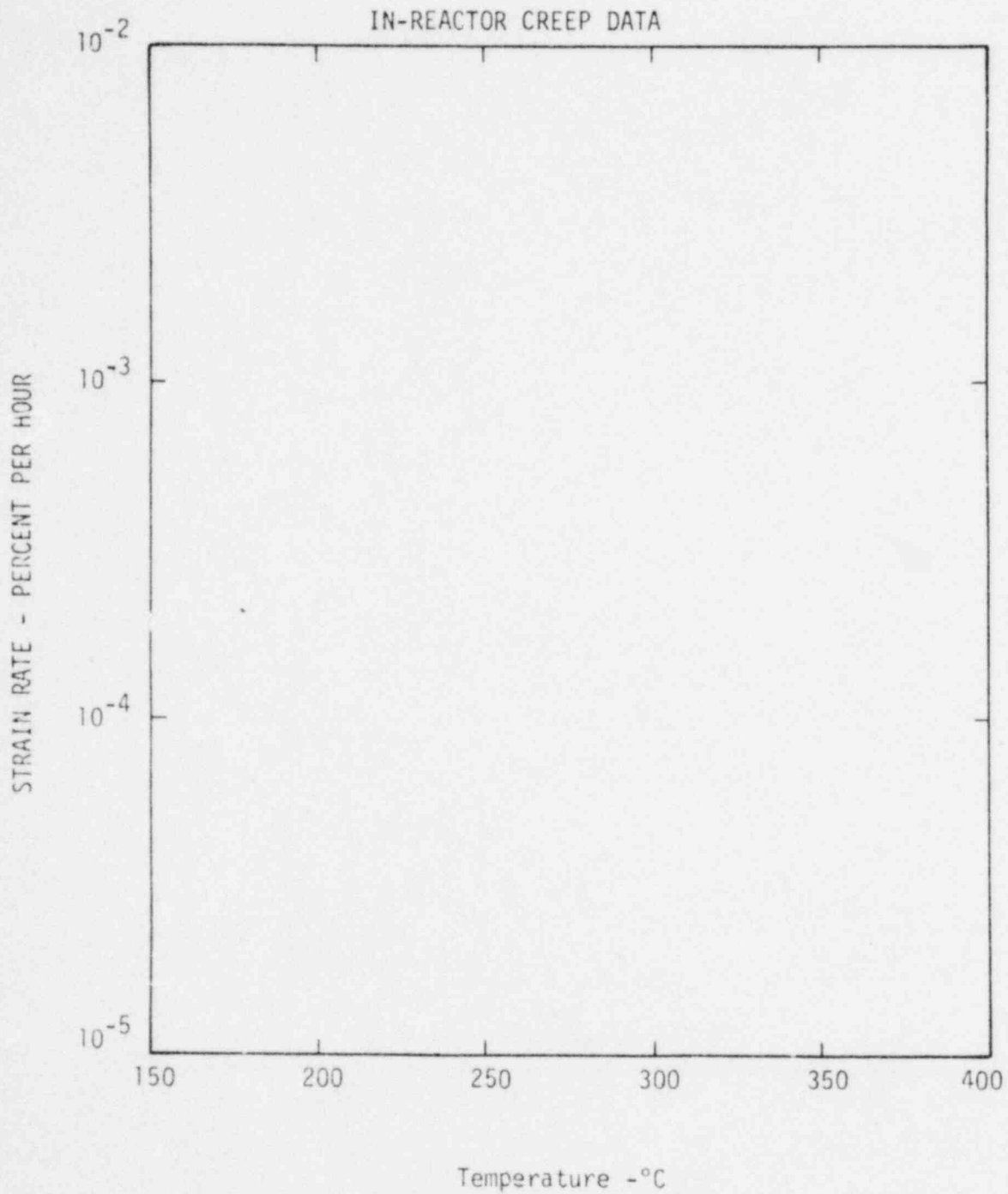


FIGURE 3-5

EFFECT OF TEMPERATURE ON
SECONDARY CREEP RATE OF ZIRCALLOY
($\sigma = 20000$ PSI)

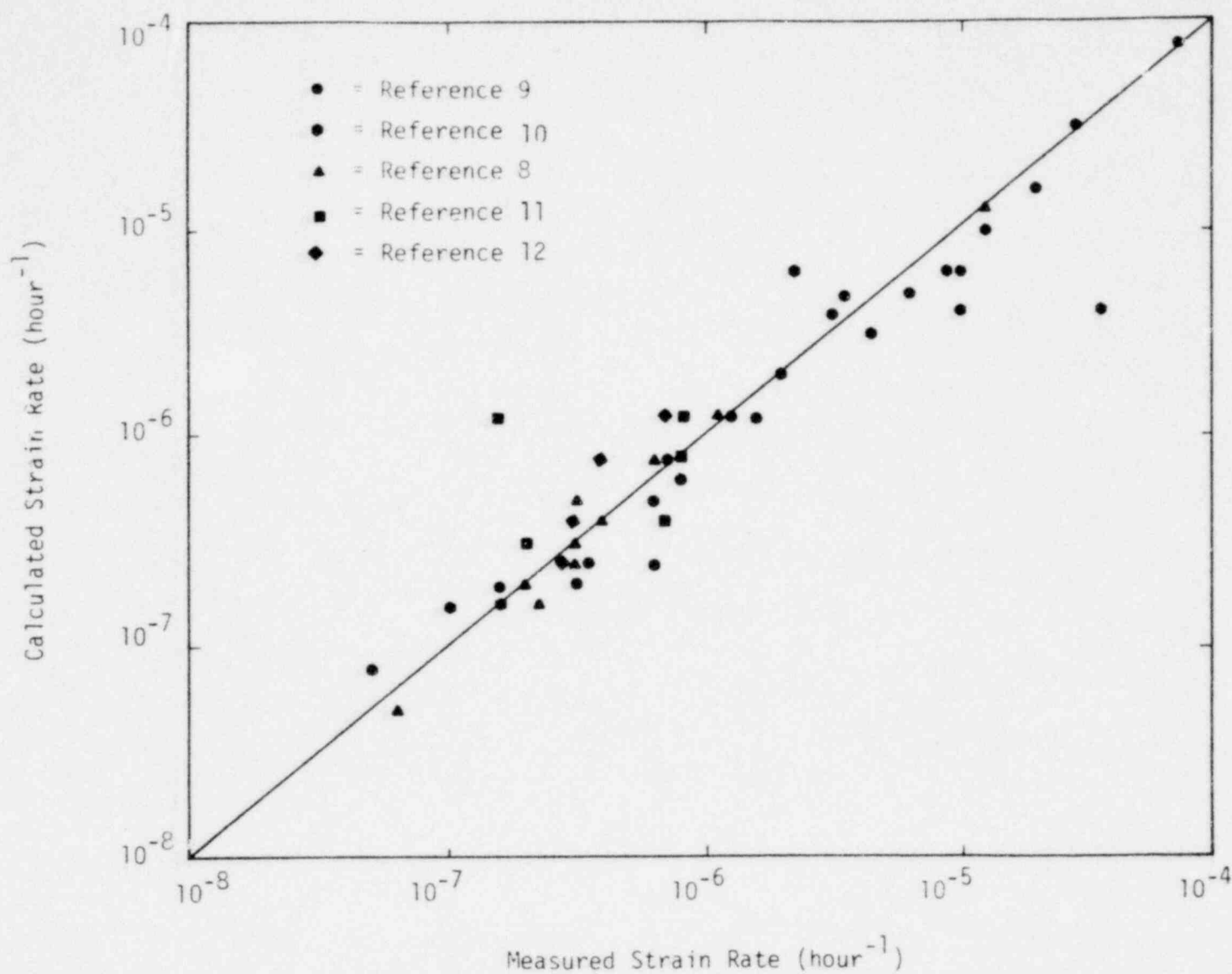


FIGURE 3-6

CALCULATED CREEP RATE VERSUS MEASURED CREEP RATE (IN-REACTOR ZIRCALOY PRESSURIZED TUBES AND TENSILE CREEP SPECIMENS)

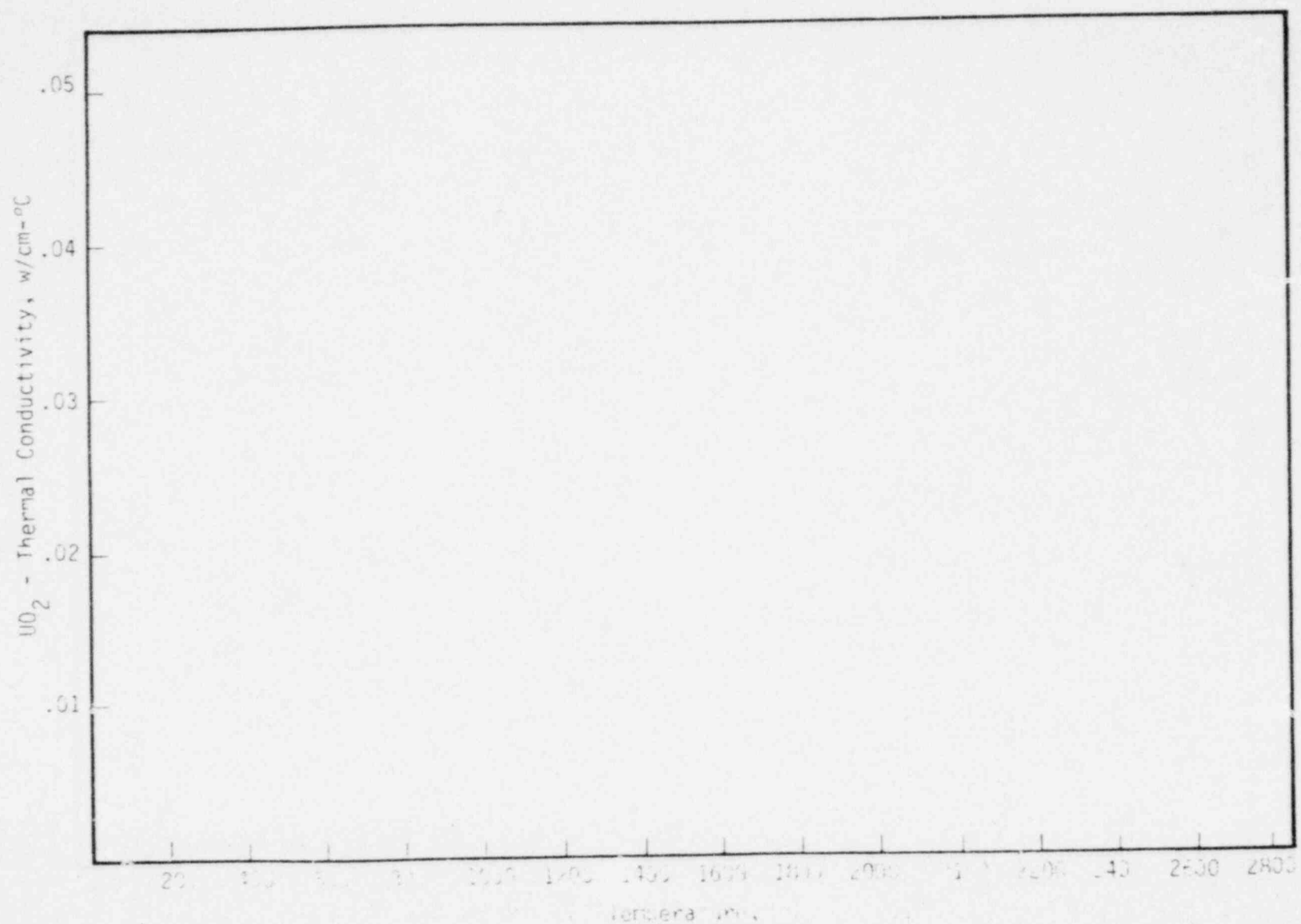


FIGURE 3-7 UO₂ THERMAL CONDUCTIVITY AS A FUNCTION OF TEMPERATURE (Reference 16)

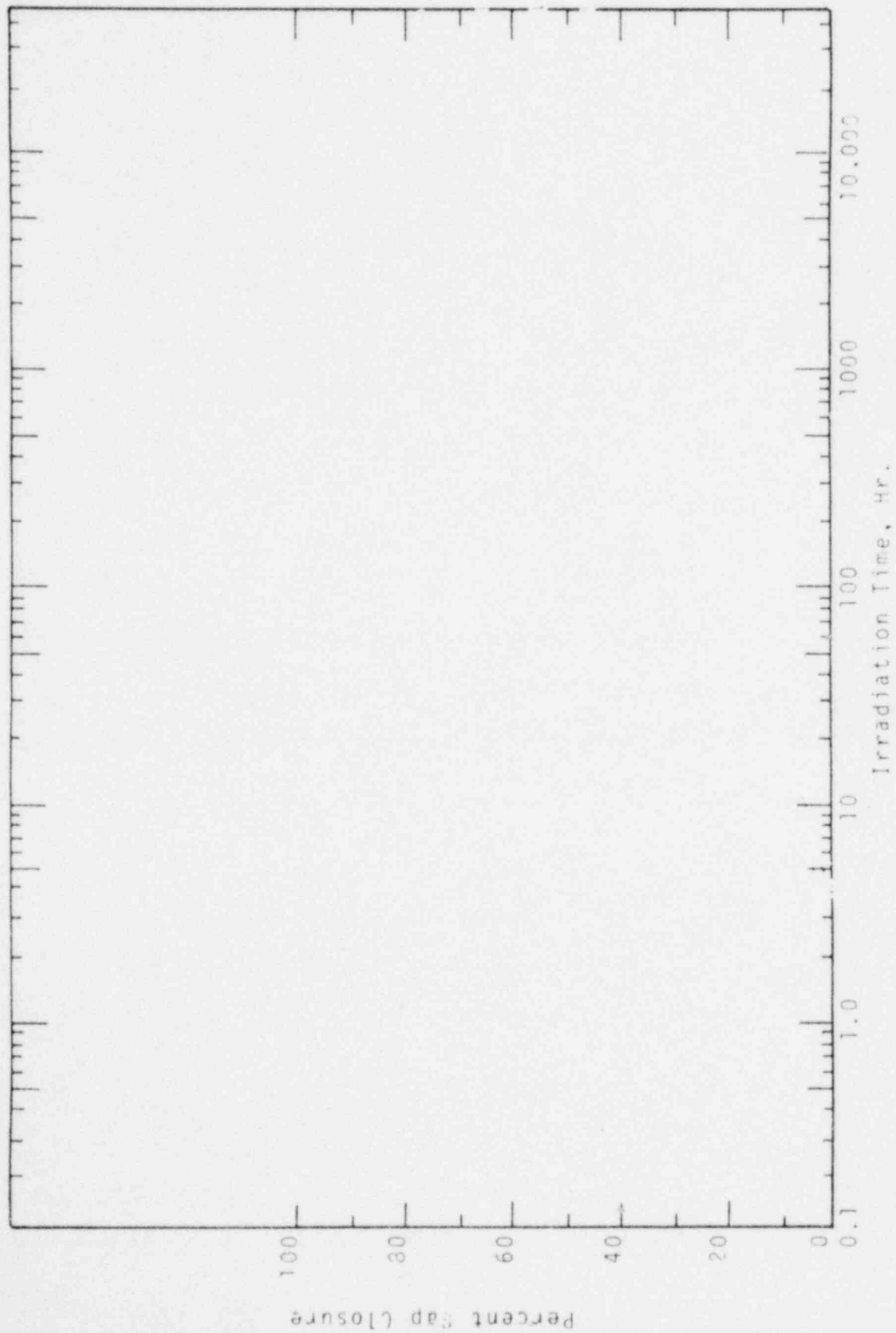


FIGURE 3-3 GAP CLOSURE OF AS-FABRICATED GAP VERSUS IRRADIATION TIME

4.0 FUEL ROD FAILURE MECHANISMS ANALYSIS

Fuel rod failure mechanisms are classified as:

1. Corrosion - Corrosion reduces the material thickness and results in less load carrying capacity. In addition, ductility decreases as Zircaloy absorbs hydrogen produced during corrosion. Fuel failure can result from hydrogen embrittlement.
2. Mechanical - Mechanical failure mechanisms can be classified as strain limited phenomena, stress limited phenomena, and creep collapse. The strain limited mechanism is most likely to be a fuel-cladding interaction which leads to failure by either axial ratchetting or local strain failures at pellet interfaces. Stress limited failure mechanisms result from incompatible internal or external pressures which lead to either rod burst or collapse, respectively. Creep collapse occurs due to separation of the pellet stack combined with reactor operating conditions that produce a high rate of cladding creepdown.
3. Mechanically Assisted Corrosion - This type of failure includes stress corrosion and fretting corrosion. These failure mechanisms are complex and can lead to fuel rod failure in shorter time than predicted for either corrosion or mechanical loading failure mechanisms acting separately.

These fuel failure mechanisms and features of the ENC fuel design that accommodate the failure mechanisms are discussed in detail in the following sections.

4.1 CORROSION FAILURE

It is well established that zircaloy corrosion rates are temperature dependent.⁽²⁷⁾ It is also apparent that irradiation increases the corrosion rate;⁽²³⁻³¹⁾ however, the irradiation effect has not been fully established. The history of fuel performance in PWR's shows a small but definite increase in corrosion rates attributable to irradiation. Under some conditions, the effect of irradiation on corrosion rate is significant but may also depend on alloy composition and environment. Even though high corrosion rates have been observed, oxidation of the clad, per se, has not been a limiting factor for estimated local cladding temperatures greater than 850°F.

Based on available data and assumed control of coolant water chemistry (e.g., halides, hydrogen, and oxygen), the post transition corrosion rate (\dot{w}) in the temperature range 575°F to 675°F (302°C to 357°C) is:⁽³¹⁾

$$\dot{w} =$$

Weight gains, corrosion allowances, (e.g., reduction in wall thickness), and hydrogen absorption can be estimated from this corrosion rate. The relationship between corrosion rate and hydrogen absorption for fuel cladding is:⁽³¹⁾

$$H_{\text{ppm}} =$$

where:

Zircaloy-4 was selected for cladding since it has a lower hydrogen absorption factor than Zircaloy-2 in a PWR environment. The reported absorption factor (f) for Zircaloy-4 in hydrogenated water ranges from

The amount of hydrogen absorbed in a fuel rod after 28,000 hours of operation (calculated with the maximum reported corrosion rate and absorption factor, minimum wall thickness, and conservative assumptions) is:

$$H =$$

4.2 MECHANICAL FAILURE MECHANISMS

4.2.1 Strain Limiting Phenomena

Cladding ductility is an important parameter in design of nuclear fuel rods. Because PWR's operate at such high pressures, high strengths are required to maintain stress limit margins. High ductility

is required to accomodate fuel thermal expansion and swelling in addition to thermal transients and power cycle shifts. The cladding must not only meet all of these requirements, but also have mechanical properties that minimize creep rates in order to prevent cladding collapse.

4.2.2 Pellet-Cladding Interaction

High localized cladding strains caused by pellet-cladding interactions can result in fuel failure. The failures occur when the fuel is held at one power level followed by a rapid increase in operating power. Localized cladding strain occurs at pellet interfaces and at pellet crack locations. Localized ductile cladding cracks are associated with circumferential ridges. If ridging is minimized, then the probability of pellet-cladding failure is reduced. Increased pellet-to-cladding gap, pellet dishing, reduced pellet length, chamfered or beveled pellet edges, and thicker cladding all reduce ridging.⁽³⁶⁾ The ENC fuel design incorporates dished, short pellets, thick cladding, and a controlled pellet-cladding diametral gap to minimize the potential of pellet-cladding interaction failures.

b) Rod Growth

Axial extension of fuel rods results from both irradiation growth and pellet-clad interaction. Excess axial extension of fuel rods can interfere with tie plates and result in rod bow and possible failure.

Irradiation growth of

tubing is based on

illustrated in Figure 4-1 and is approximately linear with fast flux

($n/cm^2 \text{ sec} > 1.0 \text{ Mev}$). ENC irradiated fuel rod and guide tube length measurements correlate well with the zircaloy growth models.

To accomodate possible ratchetting effects, the fuel assembly design allows for fuel rod extension equal to 1.0% of the fueled length; greater than predicted by The maximum predicted fuel rod extension is less than the minimum design clearance between the fuel rod end caps and the tie plates.

4.2.3 Strain Limits

The strain limits shall be as follows:

-
-

The ductility data for irradiated zircaloy which was presented in the previous section is for strain rates of 1.0% per hour or greater. Fuel swelling rates and creep strain rates due to internal fission gas pressures beyond the mid-life of the fuel are at rates of 10^{-5} to 10^{-3} per hour. Experience over the past 10 years has shown that based on total elongation, provides an acceptable margin of safety against failure.

The strain limit must be reduced when the strain rates are appreciably greater than for creep or fuel swelling. The basis for limiting high strain rate strains is to avoid exceeding the intrinsic uniform strain for the cladding material at the prevailing conditions. High rates of cladding strain are likely after fuel shuffling when fuel elements which have accumulated appreciable burnup in low power regions are moved to high power regions. At fast fluence $<10^{20}$ n/cm², the cladding can accommodate fuel shuffling; while at fluences $>10^{20}$ n/cm², fuel shuffling should be as infrequent as possible. ENC provides guidelines to utilities to minimize the potential for excessive cladding strain.

4.2.4 Stress Limiting Phenomena

a) Membrane - Steady State Stresses

The ENC cladding design criteria requires that all steady state stresses be within the American Society of Mechanical Engineer's (ASME) Section III, Boiler Code Limits⁽³⁹⁾ as shown in Table 5.1. As the cladding thickness increases, for a given cladding strength, the stress limit margin increases. Therefore, the ENC etched fuel design, with a nominal cladding thickness of 30 mils, requires less prepressurization to maintain the same stress margin as a fuel rod with a 24 mil nominal clad thickness. Stress limit margins for unetched 31 mil thick cladding are further increased. The calculation methods for the various types of membrane stresses are presented in Section 5.0.

b) Cyclic Stresses

Cyclic stresses are produced by flow-induced vibrations and reactor load-following operation. The stress limit for flow-induced vibrations, shown in Figure 4-2, is based on work reported by O'Donnel and Langer.⁽⁴⁰⁾ The vibration stress for a fuel rod is calculated from Paidoussis' analysis^(41,42) of the flow-induced vibration of cylinders in axial flow. Section 5.0 presents the detailed analysis.

Power cycling has been considered detrimental to fuel life due to potential fatigue failures. Stress is generated by: 1) pellet-cladding interactions due to loss of pellet-cladding gap from gradual creep-down of the zircaloy cladding and irradiation-induced swelling of fuel pellets, and 2) cyclic thermal gradients. Reactor power variations change contact forces and produce cyclic stresses in the cladding.

The occurrence of cyclic stresses can be delayed by reducing cladding creep-down by pressurization of fuel rods to partially offset the external pressure. ENC fuel rods are internally pressurized to reduce the creep-down rate.

The calculated strain and cyclic stresses for reactor operation are within design criteria requirements. These calculations are summarized in Section 5.0.

4.2.5 Creep Collapse

Creep collapse of PWR fuel rods occurs when: 1) the pressure, temperature, and fast flux conditions are sufficient to generate relatively high in-reactor creep rates, and 2) separation of the pellet

stack removes the support for the cladding. Pellet stack separation is attributed to fuel densification and pellet hangups. Pellet hangup is reduced by a high pellet stack preload (a spring with low irradiation induced relaxation), large diametral gaps, smooth ID cladding finishes, and tight tolerances on pellet end face perpendicularity. High initial pellet density and thermally stable pellets limit in-core densification. Thick cladding and internal prepressurization help to prevent cladding collapse if pellet stack separation does occur. The ENC fuel incorporates dished pellets with precision ground cylindrical surfaces and a high pellet stack preload to reduce pellet-cladding hangup. Thick cladding and fuel rod prepressurization reduce the probability of creep collapse. Details of the creep collapse analysis are in Section 5.0 of this report.

4.3 MECHANICALLY ASSISTED FAILURE MECHANISM

4.3.1 Stress Corrosion

Rosenbaum's analysis⁽⁴³⁾ of fuel failure was one of the earlier discussions of stress corrosion failure. Fission product iodine was suspected as the major corrosion agent and tensile stresses resulted from pellet-cladding interactions. Laboratory testing has confirmed that zircalloys are susceptible to stress corrosion cracking in an iodine vapor atmosphere.⁽⁴⁴⁾

Stress-corrosion cracking is sensitive to stress level. For any degree of pellet-cladding interaction, the stress level is reduced as cladding is increased in thickness. Therefore, the ENC

0.030 inch thick cladding has a lower susceptibility to stress corrosion cracking as compared to thinner cladding PWR fuels. In laboratory tests, Garlick⁽⁴⁴⁾ indicated that for 0.030 inch thick zircaloy cladding it was very difficult to reach stress levels sufficient to cause cracking in an iodine environment.

4.3.2 Fretting Corrosion

Fretting corrosion failure has a high potential for occurrence in an improperly designed fuel assembly due to flow-induced vibrations of fuel rods. Based upon in-reactor experience and testing of nearly identical ENC fuel assembly designs, the potential for fretting corrosion failure is very low for the proposed assembly design.

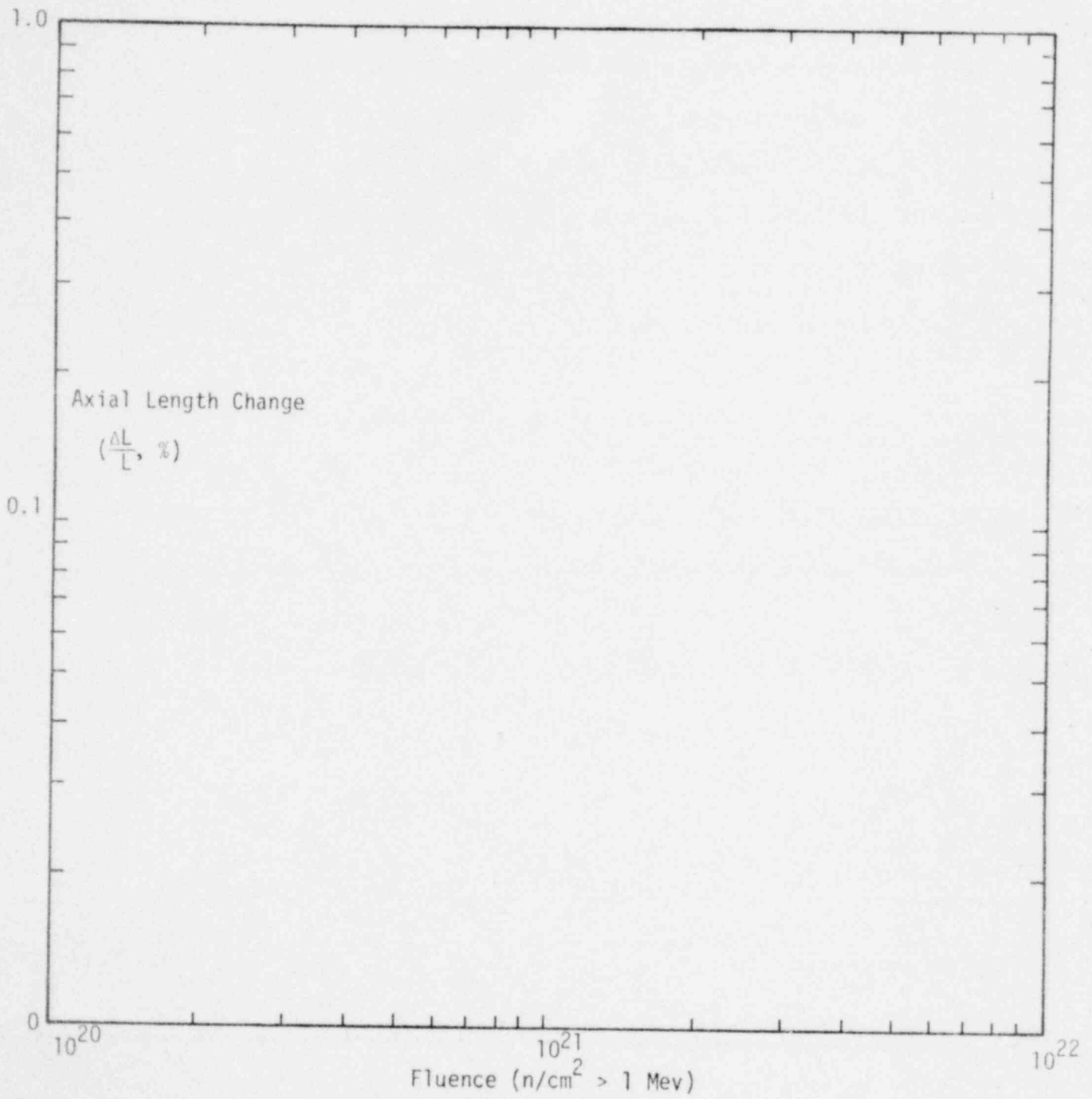


FIGURE 4-1 AXIAL IRRADIATION GROWTH OF ZIRCALOY TUBING

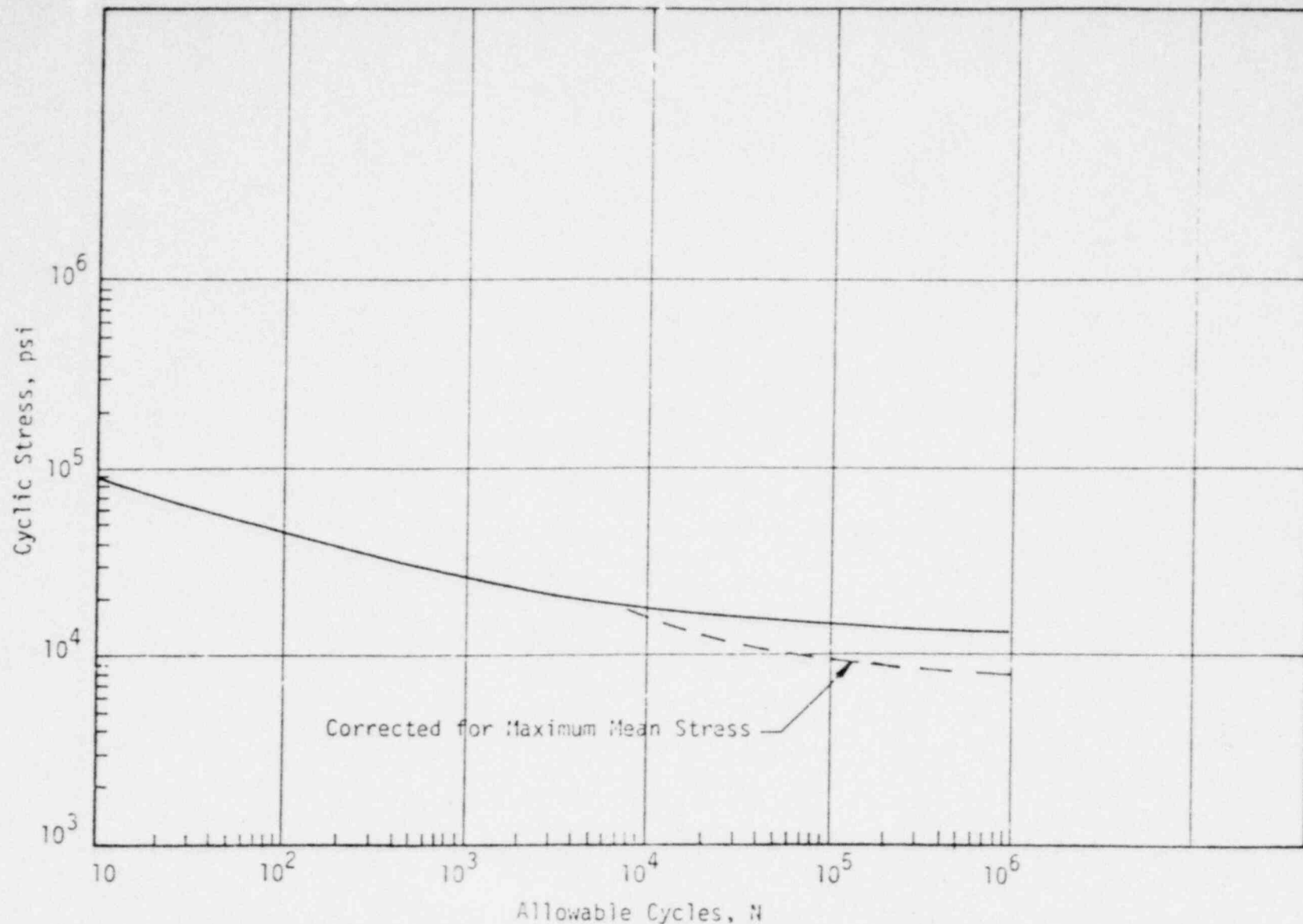


FIGURE 4-2

CYCLIC FATIGUE DESIGN CURVE FOR IRRADIATED
ZIRCALOY-2 OR -4 ROOM TEMPERATURE TO 600°F (316°C).
TOTAL IRRADIATION EXPOSURE 5.5×10^{21} nvt
FAST FLUENCE (>0.625 cV) (Reference 40)

5.0 COMPONENT MECHANICAL DESIGN ANALYSIS

This section describes the mechanical design analysis of the fuel assembly and includes: 1) fuel rods, 2) tie plates, 3) guide tube, 4) spacers, and 5) overall structure. Required material properties are summarized in Section 3.3 and material strengths are summarized in Table 3.1.

5.1 FUEL RODS

5.1.1 General Description

Standard ENC fuel rods have Zircaloy-4 cladding with 94.0% nominal density UO_2 pellets. Gadolinia burnable poison rod assemblies have pellets with up to Gd_2O_3 dispersed in a UO_2 matrix. The properties of the UO_2 are essentially unaffected by the Gd_2O_3 . Thus, the design analysis for standard fuel rods is applicable to burnable poison rod assemblies. The as-fabricated nominal diametral pellet-cladding gap is The active fuel length is 144.0 inches and the total fuel rod length is inches. The long upper plenum contains an Inconel X-750 spring. An Al_2O_3 insulator disc is placed on each end of the pellet stack. The rods are purged and prepressurized with helium, and Zircaloy-4 end caps are fusion welded to the cladding.

5.1.2 Design Criteria

Cladding

- a) Cladding must remain free standing throughout the design lifetime.
- b) Cladding stresses shall not exceed the limits described in Table 5.1.
- c) Maximum cladding strain shall not exceed (steady state) at end-of-life (EOL).

For transient occurrences, the maximum incremental strain as a function of accumulated fast fluence shall be:

- d) The cumulative usage factor for cyclic stresses shall not exceed
- e) Hydrogen absorption shall not exceed
- g) Cladding Temperatures shall not exceed:

5.1.3 Cladding Stress Analysis

Steady-State Stress Analysis

The results of the steady-state stress analysis and the appropriate stress limits are summarized in Table 5.2. The BOL calculations were based on etched 30 mil cladding wall thickness. EOL calculations assumed reduction in wall thickness to conservatively account for corrosion. The stress analysis assumed maximum fuel rod power with minimum fill gas pressure and minimum gas release. Stress intensities would be lower for wall thickness cladding.

Primary Membrane Stresses

The primary membrane stresses are produced by the coolant pressure and fuel rod fill gas pressure. The stresses are calculated by the Lamé equations recommended by P. Shariffi and E. P. Popov.⁽⁴⁵⁾

$$\sigma_{\text{hoop}} = [P_i R_i^2 - P_o R_o^2 + (R_i R_o / r)^2 (P_i - P_o)] / (R_o^2 - R_i^2)$$

$$\sigma_{\text{radial}} = [P_i R_i^2 - P_o R_o^2 - (R_i R_o / r)^2 (P_i - P_o)] / (R_o^2 - R_i^2)$$

$$\sigma_{\text{axial}} = (\sigma_{\text{hoop}} + \sigma_{\text{radial}}) / 2.0$$

where:

σ = primary membrane stress, psi

P_o = external pressure = 2250 psi

P_i = internal pressure, psi

r = any radius in the cladding, inches

R_i = internal radius =

R_o = outside radius =

Primary Bending Stresses

Bending stresses due to ovality are calculated with Timoshenko's equation. (46)

$$\sigma_{\text{hoop}} + \sigma_{\text{bending}} = \sigma_{\text{hoop}} \left[1 + \frac{6U}{t} \left(\frac{P_a}{P_a - P} \right) \right]$$

where:

σ_{hoop} = Lamé' primary membrane stress, psi

$$U = \frac{\text{ovality}}{4} = \frac{ID_{\text{max}} - ID_{\text{min}}}{4} =$$

t = minimum wall thickness =

P_a = critical collapse pressure for perfect tube, psi

$$P_a = \frac{E}{4(1-\nu^2)} \left(\frac{t}{r} \right)^3$$

$$P = P_o - P_i$$

E = Young's Modulus, psi =

T = °F

ν = Poisson's Ratio =

r = mean radius =

Secondary Stresses

Cladding Thermal Gradient Stresses

Fuel rods operate with a temperature gradient across the cladding wall which results in significant thermal stresses. Assuming no stress relaxation, thermal stresses are calculated by:⁽⁴⁷⁾

$$\sigma = \pm \frac{E \alpha (\Delta T)}{2(1-\nu)}$$

where:

E = elastic modulus at

α = coefficient of thermal expansion =
in/in/°F

ΔT = temperature gradient, °F

ν = Poisson's Ratio =

σ = hoop stress assumed equal to longitudinal stress, psi

The thermal gradient, ΔT , can be calculated by:

$$\Delta T = \frac{CQ \ln d_o/d_i}{2\pi k}$$

where:

C = conversion constant =

Q = linear heating rating, kw/ft

d_o = cladding OD =

d_i = cladding ID =

K = thermal conductivity =

Combining the above equations results in the stress equation:

$$\sigma = \frac{CE\alpha Q \ln(d_o/d_i)}{4 K(1-\nu)}$$

Restrained Thermal Bow⁽⁴⁸⁾

$$\sigma_{axial} = \pm \frac{\alpha \Delta T E}{2}$$

$$\sigma_{hoop} = \pm \frac{\alpha \Delta T E}{2(1-\nu)}$$

where:

α = thermal expansion coefficient = in/in/°F

ΔT = temperature differential around a tube assumed for design calculations to be equal to

E = Young's Modulus =

T = °F

ν = Poisson's Ratio =

Restrained Mechanical Bow

Stress from mechanical bow between spacers, assuming maximum as-built fuel rod bow is zero, is calculated by:⁽⁴⁹⁾

$$\sigma = \frac{8Er}{L^2} a$$

where:

E = Young's Modulus =

T = °F

r = outer radius =

L = distance between spacers =

a = maximum rod bow =

Flow Induced Vibration Stresses

Vibrational stress due to flow induced vibrations is calculated with the Paidoussis^(41,42) analysis which assumes the following:

The maximum vibrational stress of is evaluated with the fatigue design curve for zircaloy of O'Donnell and Langer⁽⁴⁰⁾ (Figure 4-2) corrected for maximum mean stress, and the results are included in Table 5.2.

Contact Stress From Spacer Dimples

The contact stresses at the dimple locations are determined by the for calculating local stresses in spherical and cylindrical shells due to external loading.

These

stresses are incorporated in Table 5.2.

5.1.4 Fuel Rod End Cap Analysis

General Description

Zircaloy end caps are seal welded to each end of the fuel rod cladding.

The stress analysis is applied to the lower end cap only since the maximum temperature gradients occur in the lower end cap.

Lower End Cap Design for Pressurized Fuel Rods

Calculations with the computer codes JTEMP⁽⁵¹⁾ and JSTRES⁽⁵²⁾

5.1.5 Cladding Collapse

Instantaneous Collapse

The instantaneous collapse pressure, P_c , is calculated from the equation developed by Timoshenko and Gere:⁽⁴⁸⁾

$$P_c = \frac{E}{4(1-\nu^2)} \left(\frac{t}{R}\right)^3$$

where:

E = elastic modulus at average clad temperature

=

T = °F

ν = Poisson's Ratio =

t =

R =

This equation does not account for the effect of ovality on collapse pressure. The critical pressure is determined as:

$$P_{cr} = \frac{A - \sqrt{A^2 - 4B}}{2}$$

where:

$$A = \frac{\sigma_y t}{R} + p_c \left(1 + \frac{6U}{t} \right)$$

$$B = \frac{\sigma_y t p_c}{R}$$

σ_y = minimum yield stress =

t =

R = mean radius =

$$U = \frac{\text{ovality}}{4} =$$

The critical pressure is which is more than twice the reactor operating pressure.

Creep Collapse

Collapse of fuel rod cladding may occur due to creep under external pressure. Irradiation creep of Zircaloy-4 is dependent on temperature, stress, fast neutron flux (> 1 Mev) and the metallurgical condition of the material. Cladding ovality has a significant effect on the collapse time. Parametric analyses have shown that cladding temperature and stress are the dominant parameters in creep collapse. Creep collapse is evaluated by the ENC RODEX and COLAPX codes.

The RODEX code⁽¹³⁾ predicts the cladding temperature and the internal pressure history a fuel rod based on a model which accounts for changes in plenum volume and axial variations in gap and dish volumes produced by thermal expansion, and fuel densification

and swelling. Gas absorption by pellets is also modelled in RODEX. No pellet fission gas release is assumed. The appropriate conservative options for all variables are selected for the RODEX input. The temperature and internal pressure history is input into the COLAPX code⁽⁵³⁾ which calculates, by large deflection theory, geometry changes and creep deformation of the cladding as a function of time.

The most severe collapse condition for the cladding is to have a high initial power while the densification process occurs. The design basis power history for collapse is summarized in Table 5.3.

The results of the calculations are summarized as:

cladding creep collapse is not predicted during the fuel rod design life for the corresponding design criteria batch average discharge burnup.

5.1.6 Cladding Strain Analysis

Cladding strain is evaluated by an interactive calculation procedure which considers the thermal-hydraulic environment at the cladding surface, the pressurization within the cladding, and the thermal, mechanical and compositional state of the fuel and cladding. The RODEX⁽¹³⁾ code performs these interactive calculations for conservative fuel rod power histories. In addition to evaluation of the fuel rod strain for normal operation, this code determines the initial conditions for fuel rod power ramping analyses.

The fuel rod performance characteristics modeled by the RODEX code are:

- 1) Gas release
- 2) Radial thermal conduction and gap conductance
- 3) Free rod volume and gas pressure calculations
- 4) Pellet-cladding interaction
- 5) Fuel swelling, densification, cracking and crack healing
- 6) Cladding creep deformation and irradiation induced growth

The calculations are performed on a time incremental basis with conditions updated at each calculated increment so that the power history and path dependent processes can be modeled. The axial dependence of the spatial power and burn-up distributions are handled by dividing the fuel rod into a number of fuel segments which are modeled as radially dependent regions whose axial deformations and gas release are summed. Power distributions can be changed at any desired time and the coolant and cladding temperatures are readjusted at all axial nodes. Deformations of the fuel and cladding and gas release are incrementally calculated during each period of assumed constant power generation. Gap conductance is calculated for each of these incremental calculations based on gas release throughout the rod and the accumulated deformation at the center of each axial region within the fueled region of the rod. These deformation calculations consider fuel densification, swelling and cracking, thermal expansion, cladding creep down, irradiation induced growth, and fuel creep and crack healing.

The pellet-cladding interaction during reactor operation is dependent on the power history. The peak discharge burnup fuel rod was analyzed, and the design basis power history is summarized in Table 5.3. The RODEX strain analysis for the power history are summarized as:

Based upon the design criteria and technical bases criteria of a maximum (steady-state) strain of the RODEX calculated strains are acceptable for the corresponding design criteria batch average discharge burnup.

The clad strain due to transient power changes was calculated with the RAMPEX code.⁽⁵⁴⁾ This code calculates the pellet-cladding interaction during a power ramp. The initial condition is obtained from RODEX output. The RAMPEX code considers the thermal condition of the rod in its flow channel and the mechanical interactions that result from fuel creep, crack healing, cladding creep, and cladding plastic deformation at any desired plane in the rod during the power ramp. Any plastic strain which results due to the power ramp is compared with the strain limit criteria for transient occurrences.

Transient analyses were performed for the peak discharge burnup fuel rod history summarized in Table 5.3. The fuel rods were ramped when pellet/cladding steady state strain was a maximum. At this time, maximum cladding creep down and pellet densification had occurred and resulted in maximum pellet clad interaction during the subsequent power ramp. The power was ramped

The power was increased at a

startup rate of to 100%. Although these ramp rates are not recommended as normal operating modes, they did not cause the cladding to exceed the design criteria of plastic strain for transient occurrences.

In addition to the transient strain analyses, a fatigue usage factor for the cladding was calculated. The calculations were based upon the duty cycles summarized in Table 5-4. Cladding stress values from the RAMPEX runs were for 0-100% power cycles. Fractions of these stresses were assumed for power changes of less than 100%. (55)

has shown that fuel cracks may cause stress concentrations in the adjacent cladding. To account for this effect, an assumed total strain concentration factor of applied to the calculated cyclic cladding stresses.

Table 5.5 summarizes the final cladding cyclic stresses and the fatigue usage factor. The allowable cycles for each stress amplitude were determined from the fatigue design curve for zircaloy shown in Figure 4.2 which considers the effect of maximum mean stress. The total usage factor meets the design criteria requirement of a maximum allowable cumulative usage factor of

5.1.7 Pellet Design

Short Versus Long Pellets

The ENC design incorporates short fuel pellets and is based upon analytical and experimental evidence which indicates improved performance with short pellets.

Short fuel pellets have the following advantages:

1) reduced "hourglassing" during reactor operation, 2) reduced "hourglassing" in the sintering process which results from a more uniform green pellet density, and 3) reduced pellet grinding which reduces pellet chipping and debris contamination. As evidenced from Halden experience⁽⁵⁶⁻⁵⁹⁾ as shown in Figure 5-1, the reduced hourglassing results in less pellet-cladding interaction and fuel rod elongation.

Dished Versus Nondished Pellets

- Axial Elongation

The parabolic radial temperature distribution in a fuel pellet results in a much larger thermal expansion of the center portions of the pellet as compared to the edge regions. The differential axial expansion of the pellets can be accommodated by sufficient axial clearance (plenum) at the end of the fuel stack provided that the pellets do not interact with the cladding. Thus, axial cladding elongation in a free-standing cladding is controlled by the diametral gap and a plenum to accommodate the axial movement of the fuel. Notley, et al.,⁽⁶⁰⁾ evaluated dish geometry and concluded that axial expansion was inversely related to diameter expansion as shown in Figure 5-2. The results should be interpreted in a qualitative sense because initial diametral clearances, the cladding strength, the peak heat rating, and the rate of any power changes must be known before the data can be compared with other tests.

- Circumferential Ridges

A pellet dished to the edge of the outside diameter produces the smallest axial elongation and the largest ridges. A dished-shoulder design is a compromise between a flat pellet and a fully dished pellet. The various geometries can be compared on a relative scale (three being the least desirable, as follows:

<u>Pellet Geometry</u>	<u>Axial Elongation</u>	<u>Circumferential Ridging</u>
Flat	3	1
Full Dish	1	3
Dish-Shoulder	2	2

5.1.8 Fuel Rod Bow Analysis

To date, ENC has a data base of over fuel rod-to-fuel rod and fuel rod-to-guide tube spacing measurements from inspection of irradiated ENC fuel in three (3) separate PWR's to a maximum exposure of MWD/MTU. Fuel rod-to-fuel rod spacing measurements for ENC H. B. Robinson reload fuel is presented in Figure 5.3, and fuel rod-to-guide tube spacing measurements are presented in Figure 5.4. The measurement data have been statistically reduced so that a 95/95 confidence level of fractional channel closure could be calculated. The from the bottom of an assembly consistently has the maximum fractional channel closure for the respective assembly. Fractional channel closure vs. assembly average burnup is summarized in Figure 5.5.

Thus, rod bow is expected to have minimal, if any, effect on current technical specification limits.

Special features of the ENC fuel design significantly reduce the extent of fuel rod creep bow as compared to the existing fuel design. These features include:

1. Thicker etched cladding
2. A 5 point rod support system (4 dimples and 1 spring versus 4 dimples and 2 springs) which results in less axial restraint. This feature is illustrated in Figure 5-6.
3. A deeper spacer grid which produces a higher rotational restraint on rods at spacer support points.
4. Fuel rods supported independent from upper and lower tie plates to reduce axial loads.

The AXIBOW⁽⁶¹⁾ code was developed by ENC to evaluate in-reactor fuel rod bow. The computer program is a finite element code with beam elements that have axial thrust and linear spring elements for

nodal restraints. The effect of axial thrust, creep relations, irradiation induced growth, anisotropic creep, initial curvature, temperature and flux gradients, eccentric cross sectional geometries, and axial thrust relaxation can be evaluated with the code.

Sensitivity studies were performed which included variations of axial thrust, pressure differential, initial curvature, mean cladding temperatures, neutron fast flux level, support rotational restraint, lateral temperature and flux gradients, tubing anisotropy and eccentricity, thrust relaxation, and multispan restraint. For a PWR fuel rod, the axial thrust and the support rotational restraints are the primary parameters which influence the structural stability of a fuel rod support design. Thrust relaxation and rod restraint in the various spans also significantly affects rod bow. The AXIBOW⁽⁶¹⁾ code has sufficient capability to evaluate all of the factors included in the sensitivity study and can model typical conditions for a fuel rod with multiple spans. A comparison of fuel rod bow measured on irradiated ENC H. B. Robinson fuel assemblies to fuel rod bow predicted by AXIBOW is summarized as:

Burnup (GWD/MTU)

AXIBOW Prediction

Measured Fuel Rod Bow

Comparison of the AXIBOW predicted bow with the irradiated fuel measurements indicates that the ENC AXIBOW analytical prediction methods are conservative.

5.2 TIE PLATES

5.2.1 General Description

The upper tie plate assembly is the upper structural component of the fuel assembly and locates the upper end of the assembly relative to the upper reactor core plate. The upper tie plate assembly is a cast grid structure and a holddown spring system. The holddown spring system is four (4) sets of double leaf springs designed to apply a nominal holddown load of approximately

Double leaf springs give more deflection capability without yielding than is possible with a single leaf design. This extra spring compliance makes the spring design less sensitive to

dimensional tolerance stackups. All upper tie plate assembly parts, with the exception of the springs and their retaining cap screws, are type 304L stainless steel. The springs are Inconel 718 and the cap screws are Inconel 600.

The lower tie plate is a machined 304L stainless steel casting, controls the coolant flow to the fuel assembly, and functions as the bottom structural component for the fuel assembly.

5.2.2 Design Criteria

Strength

The strength of the upper and lower tie plates shall be sufficient to withstand reactor holddown forces, hydraulic forces, differential thermal expansion forces, and handling and transport forces. The dynamic loads for vertical handling shall be assumed to be times the dry bundle weight.

The strength of the upper and lower tie plates has been verified by structural testing. Previous static testing of nearly identical designs confirmed that the tie plates will withstand times the dry bundle weight in both tension and compression without measurable plastic deformation.

Dimensions

The dimensions of the tie plates shall be consistent with the thermal hydraulic flow requirements, the strength requirements, fuel handling mechanisms, and the envelope requirements

as specified in the design criteria. The tie plate configuration shall be consistent with the mating surfaces of the reactor core support system and the reactor control rod cluster and drive mechanism.

Removability

The upper tie plate shall be designed with a positive locking mechanism to allow removal from and reattachment to the fuel assembly. With the upper tie plate removed, fuel rods can be inspected and/or replaced.

Holddown Load

The holddown springs must provide a nominal holddown load on a fuel assembly to prevent levitation under normal operating conditions. The springs shall have an operating length range to accommodate differential thermal expansion and still maintain sufficient holddown forces.

Corrosion Resistance

Components shall be sufficiently corrosion resistant to provide the required design functions throughout life.

5.2.3 Holddown Spring Analysis

Holddown forces to prevent hydraulic lifting of the fuel assembly are supplied by four (4) cantilever leaf spring assemblies. The spring assemblies are depressed by the upper core plate when closing

which are within the design yield stress limits for Inconel 718.

5.3 GUIDE TUBE

5.3.1 General Description

The control rod guide tubes in the fuel assembly provide channels for the control rods during insertion and withdrawal. The guide tubes are fabricated from a single piece of Zircaloy-4 tubing drawn to two (2) different diameters. The larger diameter section at the top provides a relatively large annular area for rapid RCC insertion during a reactor trip and accommodates a small amount of upward cooling flow during normal operations.

The bottom section of the guide tubes produces a dashpot action to deaccelerate a dropped control rod during a reactor trip. The reduced diameter section at the dashpot is conical shaped for a smooth transition in diameter.

Flow holes just above the transition permit cooling water to enter during normal operation and allow water flow out of the dashpot during a reactor trip.

5.3.2 Design Criteria

With the guide tubes, spacers, and tie plates assembled into a framework, the guide tubes and attachment hardware provide, throughout the design life of the fuel assembly, adequate strength to support the weight of the fuel assembly, support the hold-down forces, resist forces from fuel rod-guide tube differential thermal expansion, and provide channels for control rod insertion.

The guide tube design shall provide for (1) sufficient coolant flow to cool the absorber rod at any insertion distance, (2) a maximum scram time of 1.8 seconds from signal initiation to control rod entry into the dashpot region, and (3) damping the control rods such that the control rod assembly spring shall not be deflected more than 0.75 inch beyond the preload condition during a scram.

5.3.3 Mechanical Design Analysis

The guide tubes, along with the upper and lower tie plates and spacers, provide the structural framework for the fuel assembly. Guide tubes are considered as restrained columns and are

analyzed with appropriate load combinations. Column deflection is permissible within allowable bending stress constraints, displacement, and approach to column instability. The total stress allowed, primary plus bending, is equal to the yield strength of the material at the temperature of the load conditions.

As the power level of the reactor increases, differential thermal expansion between the zircaloy guide tubes and the hotter zircaloy clad fuel rods puts the guide tubes in tension. Therefore, there is no concern as to the stability of the guide tubes on approach to normal operating conditions. After a period at power, vibration loads tend to reduce or eliminate differential thermal expansion loads. With a reduction in power, differences in temperature between the guide tubes and fuel rods decreases and causes compression loading on the guide tubes. Thus, the elastic stability of the zircaloy guide tubes is of most concern as the power level is reduced.

The magnitude of guide tube loading depends, partially, upon whether or not the fuel rods slip through the spacers. For slip to occur, differential thermal expansion between the guide tubes and the fuel rods must be sufficient to overcome the break-away frictional forces of the spacer contacts. If no slip occurs, the loading is one-third or less than the case where all fuel rods move through the spacer since a single span can then accumulate forces. Considering the compliance available in the zircaloy guide tubes, an effective temperature difference on the

order of 100°F between the fuel rod cladding and guide tubes might be required at full power to cause slip at spacer locations upon decrease in power. Thus, it is uncertain whether significant slip will occur. For the sake of conservatism, it is assumed that sufficient temperature gradients develop for the fuel rods to slip through all but the central spacer.

Axial loading of guide tubes by spacer-fuel rod interaction through differential thermal expansion may be cumulative over more than one (1) spacer interval. The fuel assembly guide tubes and spacers form a rigid skeleton through which the fuel rods slide against the frictional resistance of springs and dimples in the spacer grid. It is assumed that external loads are transmitted through the fuel assembly via the guide tube - tie plate framework without acting on the fuel rods. Since the fuel rods are suspended from the spacer grids without reaction at the tie plates, the forces on the fuel rods must be in equilibrium with the reactions at the spacers. A force center point where axial thermal forces are at a maximum may be assumed at the central spacer. At the central spacer, the maximum axial force per fuel rod will be the sum of the frictional resistances to sliding of the fuel rod through three (3) grid spacers in the fuel assembly. The force transmitted to the fuel rods is estimated by:

$$F_R =$$

where:

Rod loading tests with similar prototype spacer assemblies confirmed this calculated value of F_R . The average load to push a rod through a spacer cell was _____ as compared _____ assumed above.

The force applied to a guide tube during a temperature transient is:

$$F_G =$$

At BOL (cold conditions), the assembly holddown springs exert a force less than _____. This results in an additional load per guide tube. The total load per guide tube would be _____.

The column stability is defined by Euler's column formula: (48)

$$P_c = \frac{C \pi^2 EI}{L^2}$$

where:

P_c = allowable axial compressive load (lbs)

C = coefficient dependent on column end conditions
($C = 4.0$ for fully restrained ends)

L = span between spacers =

I = moment of inertia of column cross section =

E = modulus of elasticity =

$T = ^\circ F$

therefore:

$$P_c =$$

The above critical loads are significantly above the design load.

In actual practice, an initially bowed column bows an increasing amount as a compression load is applied rather than suddenly collapsing as the critical load is reached. As a result, the design load limit for a typical guide tube is more likely to be that which produces a bow unacceptable from a thermal hydraulic standpoint rather than the load which produces column instability.

The total guide tube bow may be determined by:⁽⁴⁸⁾

$$\delta = \frac{\delta_o}{1 - P/P_c}$$

where:

$$\begin{aligned}\delta_o &= \text{typical initial deflection} = \\ &= \text{total maximum deflection with an applied} \\ &\quad \text{load } P = \\ P_c &= \text{critical load as previously determined by} \\ &\quad \text{Euler column formula} = \\ \delta &= \end{aligned}$$

The resulting deflections are satisfactory from a thermal-hydraulic standpoint.

5.3.4 Hydraulic Design Analysis

The guide tube assemblies are designed to match the hydraulic conditions of the in-reactor Westinghouse fuel. The ID dimensions and location of the dashpot agree with the dimensions of the Westinghouse guide tubes. To prevent crud buildup in the lower portion of the guide tubes, the lower end fitting has a small axial hole to allow for flow. Each guide tube has four (4) weep holes for outward flow of water during control rod damping. The flow hole in the lower fitting and the weep hole diameters are sized on the basis of control rod cluster drop tests for other ENC PWR fuel designs with corrections for the geometry. The criteria for the guide tube design were as designated in Section 5.3.2:

1. Provide adequate cooling
2. Assure that time for control rods to reach dashpot location under scram conditions does not exceed 1.8 seconds

3. Upon impact of control rod cluster, the control rod assembly spring shall not be deflected more than 0.75 inch.

The velocity of the control rod assembly is limited by the forces associated with the hydrodynamic and mechanical drag which oppose the downward acceleration of the control rods. The hydrodynamic drag becomes particularly important in the dashpot region. The guide tube design provides for a rapid control rod insertion time and a low settling velocity.

The control rod assembly is rapidly deaccelerated upon entering the dashpot. The dashpot is designed to rapidly reduce the control rod velocity without excess internal pressure that could rupture the guide tube. To accomplish these objectives, the dashpot design is stepped. The length of the dashpot and the inner diameters are such that a low magnitude pressure pulse is generated as the control rod assembly is decelerated.

The burst pressure for the guide tube dashpot region is calculated as:⁽⁴⁹⁾

$$P = 2 S_u \frac{R_o - R_i}{R_o + R_i}$$

where:

P = burst pressure

R_o = external radius =

R_i = internal radius =

S_u = ultimate tensile stress

For conservatism, the analysis was for minimum strength at elevated temperature.

$$P_{burst} =$$

This burst pressure of exceeds the maximum pressure of conservatively calculated for reactor control rod insertion during a scram condition.

The pressure, drop times, and impact velocity calculation methods have been verified by testing similar ENC guide tube designs.

Rod insertion times to the dashpot were conservatively calculated to be less than seconds which is less than the minimum allowed insertion time of 1.8 seconds as stipulated in the technical specifications.

5.4 GRID SPACERS

5.4.1 General Description

The spacers are an interlocking rectangular grid of Zircaloy-4 strips. Inconel 718 spring strips are mechanically secured within the strips. Three (3) of the seven (7) spacers have mixing vane tabs to provide flow mixing to be compatible with the existing fuel. The spacers are supported by the 16 guide tubes to which they are resistance welded.

Springs and dimples are positioned within each spacer cell such that each fuel rod is in contact with one (1) spring and four (4) support dimples. The spring is a shallow arch with convolutions; it is

The Zircaloy-4 structural strips are welded at all intersections and to the side plates.

5.4.2 Design Criteria

The spacers mechanically restrain the fuel rods at seven (7) axial locations with a spring-rigid dimple arrangement to maintain a minimum spacing between rods so that the entire length of each rod can be adequately cooled. The spring force holds the rod against the rigid support dimples to prevent flow-induced vibration fretting. Each spacer also provides a lateral support to keep the rod relatively straight even if slightly bowed in its unrestrained condition.

Axial Spacing Criteria

The spacers must be axially positioned to prevent unacceptable lateral bowing of a fuel rod between spacers. Lateral rod bowing can be produced by flow induced vibrations, axial compression forces, the combined effects of a variable circumferential temperature distribution, creep bow, and an initial fuel rod bow. Regardless of the cause of bowing, the smaller the span length between grids, the smaller the bow deflection will be. The spans for the ENC fuel assembly were designed to maintain compatibility with existing fuel assemblies in the reactor core.

Spring Design Criteria

The lateral stiffness of each spacer-rigid dimple support must force a vibration node at that level. When the fuel rods vibrate, the lateral deflection amplitude at the rod midspan should be much greater than at the spacer location.

The spring must be flexible enough to elastically accommodate manufacturing tolerances and deflections during assembly and fuel rod diameter changes to a maximum of one percent during the design life. These requirements must be met without exceeding the working deflection span of the spring which is equal to the lateral displacement by a fuel rod from contact with the support dimples to contact with the backup lobes on the springs.

A minimum spring force is required to prevent fretting and to suppress thermal and as-fabricated fuel rod bow. The maximum spring force

unacceptable fuel rod scratching during assembly. In addition, the frictional load in the spacer due to the fuel rods sliding during differential thermal expansion must not overstress either the spacer structure or guide tubes or cause unacceptable creep bow of the fuel rods. Irradiation-induced relaxation of springs must also be considered in calculating the minimum spring force.

5.4.3 Spring Characteristics

Load Deflection

The load deflection characteristics shown in Figure 5-8 are from tests on production and prototype spacer springs.

Due to spacer cell and fuel rod diameter tolerance stackup, spring deflection ranges from

From the

curves in Figure 5-8, the BOL spring force ranges from

The average spring rate over this range is

Spring Rate Evaluation

The support stiffness required to force a node at a support level is generally considered to be five (5) times the simple span stiffness. That is:

$$K_{\min} =$$

where:

$$K_{\min} = \text{support stiffness required to force a node}$$

$$EI = \text{bending stiffness of fuel rod}$$

$$L = \text{minimum span length} =$$

The required stiffness for a zircaloy tube
with a wall thickness at a temperature of is:

$$K_{\min} =$$

This condition is easily met with the reference design since the support dimples are very stiff. The support stiffness is given by:

$$K_{\text{sup}} = 2K_D + K_s$$

where:

K_D = lateral stiffness of one level of support dimples

K_s = spring stiffness

The dimple stiffness was determined from experimental mechanical tests and shown to be With a nominal spring rate of the support stiffness is:

$$K_{\text{sup}} =$$

The support stiffness is much greater than the required stiffness.

Acceptability of Minimum Spring Force

The spring force, F_{v_1} , required to counteract the maximum flow vibration lateral acceleration forces to prevent the fuel rod from lifting off from both dimples simultaneously is given by:

$$F_{v_1} =$$

where:

S_v = amplitude of flow induced vibrations at rod midspan
calculated from Paidoussis's equation =

EI = bending stiffness of clad

=

L = minimum span length

=

F_{v1} =

F_{v1} =

The zircaloy fuel rods are expected to relax at a significantly greater rate than the springs, and complete relaxation of the fuel rod is expected by EOL. Therefore, only loading sufficient to overcome flow-induced vibration loads is required at EOL. With a minimum initial load of irradiation-induced spring relaxation of would be permissible. Current irradiation data indicates relaxation values on the order of at EOL as shown in Figure 5-7.

At BOL, the spring force, F_{v2} , required to prevent liftoff from one (1) dimple while rocking on the other dimple, (the mode pictured in Figure 5-9) is calculated by:

F_{v2} =

where:

δ = flow induced vibration amplitudes =

b = dimple spacing =

K_D = support dimple stiffness =

Therefore:

$$F_{v_2} =$$

The unrestrained fuel rod bow is due to manufacturing tolerances (mechanical bow) and diametral temperature differences during operation (thermal bow). The net free curvature is the sum of these effects:

$$1/R = 1/R_M + 1/R_T$$

where:

$$1/R_M = \text{mechanical curvature}$$

$$1/R_T = \text{thermal curvature}$$

If the restrained rod contacts all support dimples, it must be essentially straight. The moment in the rod required for zero restrained curvature is:

$$M = EI/R$$

Referring to Figure 5-9, the moment on the end of the rod at incipient liftoff at the upper dimple of the top support is equal to $Fb/2$. If the free curvature is uniform along the rod, this moment imposed at the top and bottom grids will make the rod completely straight, and it will contact all support points. If the curvature varies along the rod but remains the same sign, the required spring force at the interior grids will be non-zero. An upper limit on the required spring force is:

$$F_{D_2} = (2/b) EI/R_{\max}$$

where:

$$1/R_{\max} = \text{maximum free curvature along the span}$$

The mechanical bow is limited to
for a fuel rod. Assuming a circular bow, the corresponding
radius of curvature is:

$$R_M = L^2 / 2S_m$$

where:

L = length of rod =

S_m = mechanical bow =

therefore:

$$R_M =$$

The radius of curvature due to a temperature difference
 ΔT between diametrically opposed points in the cladding is:

$$R_T = d / (\alpha \Delta T)$$

where:

d = cladding diameter

α = coefficient of thermal expansion of the cladding

In the fuel rod cladding, the maximum radial temperature difference
is estimated to be The coefficient of thermal expansion of Zircaloy-4
is

$$R_T =$$

The maximum free curvature is then:

$$1/R_{\max} = 1/R_M + 1/R_T$$

$$1/R_{\max} =$$

and the required spring force is:

$$F_{D_2} =$$

To require contact at each support dimple is overly conservative since one (1) dimple in contact at each grid level will still be a stable configuration. For this condition, the support stiffness is $K_{\text{SUP}} = K_D + K_S =$ which is still much greater than K_{min} . Thus, the minimum spring force from a bowing consideration is that force required to maintain contact at one (1) dimple of each spacer. Contact at each spacer also limits mid-span bowing deflection.

The spring force required for contact at a single dimple at each spacer level is estimated on the basis of the model shown in Figure 5-10. The bow is assumed to be symmetrical with respect to the center spacer. The minimum spring force, assuming uniform curvature, is defined as F_{D_1} .

$$F_{D_1} =$$

where:

Therefore:

$$F_{D_1} =$$

$$F_{D_1} =$$

The total minimum required spring force to maintain contact at one (1) dimple per spacer is conservatively taken to be the higher F_{v_1} and F_{v_2} plus F_{D_1} , giving:

$$F_{min} = F_{v_{max}} + F_{D_1} =$$

The minimum BOL spring force of meets this requirement with ample margin.

5.4.4 Structural Integrity

Figure 5-11 illustrates two types of spacer loading that could potentially occur during reactor refueling. In one case, the assembly being placed in the core is supported by spacers on two (2) adjacent assemblies. Another possible case is restriction of assembly motion by an adjacent assembly and a core baffle. The static load on the edge of a spacer could be in the order of one-half the bundle weight in water. Impact loading could increase the effective loading but should not double it.

Edge loading tests on 14x14 PWR production spacers⁽⁶²⁾ have been performed. The tests were on two (2) 14x14 production spacer assemblies and were performed with a piece of fuel rod cladding in each cell to simulate a fuel assembly spacer. One of the spacers was hydrided

before the tests to simulate embrittlement expected in-reactor. The structural test setup is illustrated in Figure 5-12. An analysis of 15x15 PWR spacers with the STRESS-II⁽⁶³⁾ computer code showed that the structural test⁽⁶⁴⁾ stresses were comparable to in-reactor edge loading if equal individual loads are applied to the spacer edges during the tests. The highest stressed points during the tests had moments which were 10% higher than for the in-reactor case.

The 14x14 spacers were edge loaded up to (approximately times assembly weight) with deflection of selected spacer locations recorded each pounds.

Based upon the test results, the spacer strength is considered adequate to resist potential spacer edge loading during in-reactor fuel handling operations.

5.5 FUEL ASSEMBLY OVERALL STRUCTURE

5.5.1 General Description

The fuel assembly design incorporates a 14x14 square array with 179 fuel rods, 18 guide tubes and one (1) instrumentation tube. Seven (7) Zircaloy spacers with Inconel springs are positioned

along the length of the fuel assembly. The spacers are welded to the guide tubes and mechanically attached to the upper and lower tie plates. The spacers, guide tubes and tie plates form the structural framework of the fuel assembly.

5.5.2 Design Criteria

The mechanical design criteria for the fuel assembly are as follows:

Compatibility

The ENC fuel assemblies are designed to be dimensionally and structurally compatible with existing fuel assemblies in the reactor core. The locating holes on the tie plates must match locating pins on the core support and holddown structures. The upper tie plates shall be marked to visually identify the orientation of the fuel assembly in the reactor core.

Fuel Column Position

The vertical position of the fuel column in each fuel rod of each fuel assembly shall be compatible with existing fuel and the operating range of the control rods in the reactor. The nominal height of the lower end of the fuel column at room temperature shall be inches above the bottom of the lower tie plate.

Envelope

The assembly shall pass through an envelope described by a right parallelepiped 7.803 inch square. The diagonal dimension of an assembly at any cross-section shall be less than 10.870 inch. The overall assembly length shall be 159 , excluding the holddown springs.

Fuel Rod Removability

The upper tie plate shall be designed with a positive locking mechanism to allow removal from and reattachment to the fuel assembly in the refueling pool. With the upper tie plate removed, fuel rods can be inspected and/or replaced. After reattachment of the upper tie plate, the fuel assembly can be reinserted into the reactor core.

Tie Plate - Fuel Rod End Cap Spacing

The clearance between the upper and lower tie plates and the fuel rod end caps shall be a minimum of of the active fuel length.

Handling Loads

Before, during, and after the design lifetime exposure, the fuel assembly shall be capable of withstanding all normal loads from fuel handling operations without permanent deformation or distortion.

5.5.3 Design Analysis

Mechanical Integrity

The mechanical integrity during fuel assembly handling was evaluated by strength testing the guide tube to upper tie plate locking mechanism.⁽⁶⁵⁾ The test was performed on hydrided components to simulate in-reactor conditions.

Tests on individual prototypic samples showed

Based upon these test results, the locking mechanism design is considered adequate.

Fuel Assembly Fretting Potential

ENC has run fretting-corrosion tests on prototype PWR assemblies and prototype BWR assemblies. Although these tests cover wide variations in design, the design philosophy and design details for fuel rod support are substantially the same in most cases. Test periods ranged from _____ at reactor conditions of temperature, pressure and flow. Fuel rod wear depths at spacer contact points has typically ranged from _____ although wear of up to _____ in depth has been occasionally observed. Examination indicates that the wear is due primarily to fuel rod loading and unloading and not fuel rod motion during the test. There has been little or no difference between observed wear for _____ hour tests. No active fretting corrosion has even been observed on any test rod in spite of the fact that spacer springs have been relaxed up to _____ in several test assemblies.

Examination of a large number of irradiated rods has not revealed wear significantly different from that observed after loop tests. Due to the similarity with fully tested designs, no long term fretting corrosion tests are expected for this design.

Fuel Dimensional Analysis

Fuel assembly compatibility and orientation requirements have been met through dimensional analysis. Critical dimensions have been met through dimensional analysis and are identical to those of existing fuel assemblies to assure compatibility.

TABLE 5.1
STEADY STATE STRESS DESIGN LIMITS⁽³⁹⁾

Stress Category*	Stress Intensity Limits**	
	Yield Strength	Ultimate Tensile Strength
General Primary Membrane	$2/3 \sigma_y$	$1/3 \sigma_u$
Primary Membrane Plus Primary Bending	$1.0 \sigma_y$	$1/2 \sigma_u$
Primary Plus Secondary	$2.0 \sigma_y$	$1.0 \sigma_u$

* Characteristics of the stress categories are defined as follows:

- a) Primary stress is a stress developed by the imposed loading which is necessary to satisfy the laws of equilibrium between external and internal forces and moments. The basic characteristic of a primary stress is that it is not self-limiting. If a primary stress exceeds the yield strength of the material through the entire thickness, the prevention of failure is entirely dependent on the strain-hardening properties of the material.
- b) Secondary stress is a stress developed by the self-constraint of a structure. It must satisfy an imposed strain pattern rather than being in equilibrium with an external load. The basic characteristic of a secondary stress is that it is self-limiting. Local yielding and minor distortions can satisfy the discontinuity conditions of thermal expansions which cause the stress to occur.

** The stress intensity is defined as twice the maximum shear stress and is equal to the largest algebraic difference between any two of the three principal stresses.

TABLE 5.2 SUMMARY OF LIMITING STRESS INTENSITY CONDITIONS

		Stress Intensity (psi)	Design Limit (psi)	Ratio of Stress Intensity to Design Limit
1.	<u>Primary Membrane Stresses</u>			
	(Design Limit is lower value of $2/3 \sigma_y$ or $1/3 \sigma_u$.)	BOL Cold BOL Hot EOL Hot		
2.	<u>Primary Membrane Plus Primary Bending</u>			
	(Design limit is lower value of $1.0 \sigma_y$ or $1/2 \sigma_u$.)	BOL Cold - (Max. ovality) BOL Hot - (Max. ovality) EOL Hot - (Max. ovality)		
	(Stresses included in this category are the general membrane and ovality stresses.)			
3.	<u>Primary Plus Secondary</u>			
	(Design Limit is lower value of $2.0 \sigma_y$ or $1.0 \sigma_u$.)	BOL Cold BOL Hot EOL Hot		
	(Stresses included in this category are the stresses from item 2 above, plus thermal gradient, mechanical bow and spacer contact pressure.)			
4.	<u>Vibration</u>			
	(Design limit is fatigue (40) endurance limit	Flow induced		

TABLE 5.3^(a)FUEL HISTORYDESIGN BASIS FOR FUEL ROD PREPRESSURIZATIONANDCLADDING COLLAPSE AND STRAIN CALCULATIONS

<u>Cycle</u>	<u>EC. Time</u> <u>(hr)</u>	<u>LHGR</u> <u>(kw/ft)</u>	<u>Fast Flux</u> <u>(x10¹³ n/cm²-sec)</u>	<u>Rod Burnup</u> <u>(MWD/MTU)</u>
5	694	8.10		
	2776	8.30		
	5552	8.45		
	8134	8.34		
6	9492	7.90		
	12208	7.80		
	16282	7.70		
7	17609	6.70		
	20264	6.71		
	24299	6.74		

(a) Based upon Extended Burnup Power History
for Peak Discharge Burnup Fuel Rod.

TABLE 5.4DUTY CYCLES

1. Testing

Monthly valve operating test

2. Load Follow

Daily load follow for two months per year

3. Infrequent Operations

a)

b)

c)

d)

e)

f)

TABLE 5.5
CYCLIC STRESS SUMMARY

<u>Duty Cycle</u>	<u>Stress Amplitude (a) (psi)</u>	<u>Actual Cycles (b) n_i</u>	<u>Allowable Cycles N_i</u>	<u>Usage Factor n_i/N_i</u>
1		36		
2		180		
3A		3		
3B		6		
3C + 3D		24		
3E		6		
3F		144		

(a)

(b) Over 3 operating cycles.

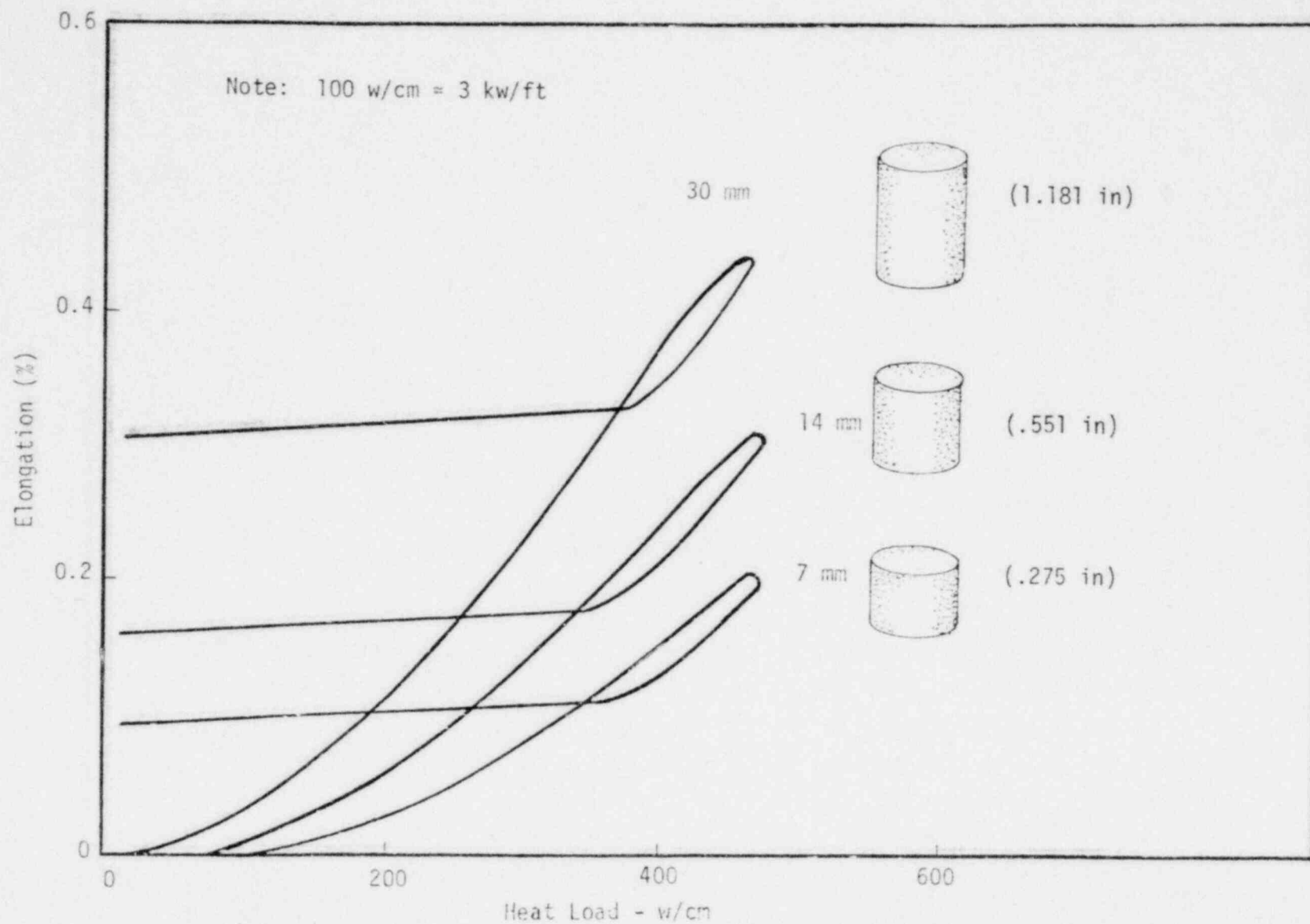


FIGURE 5-1 INFLUENCE OF PELLET LENGTH ON ROD ELONGATION

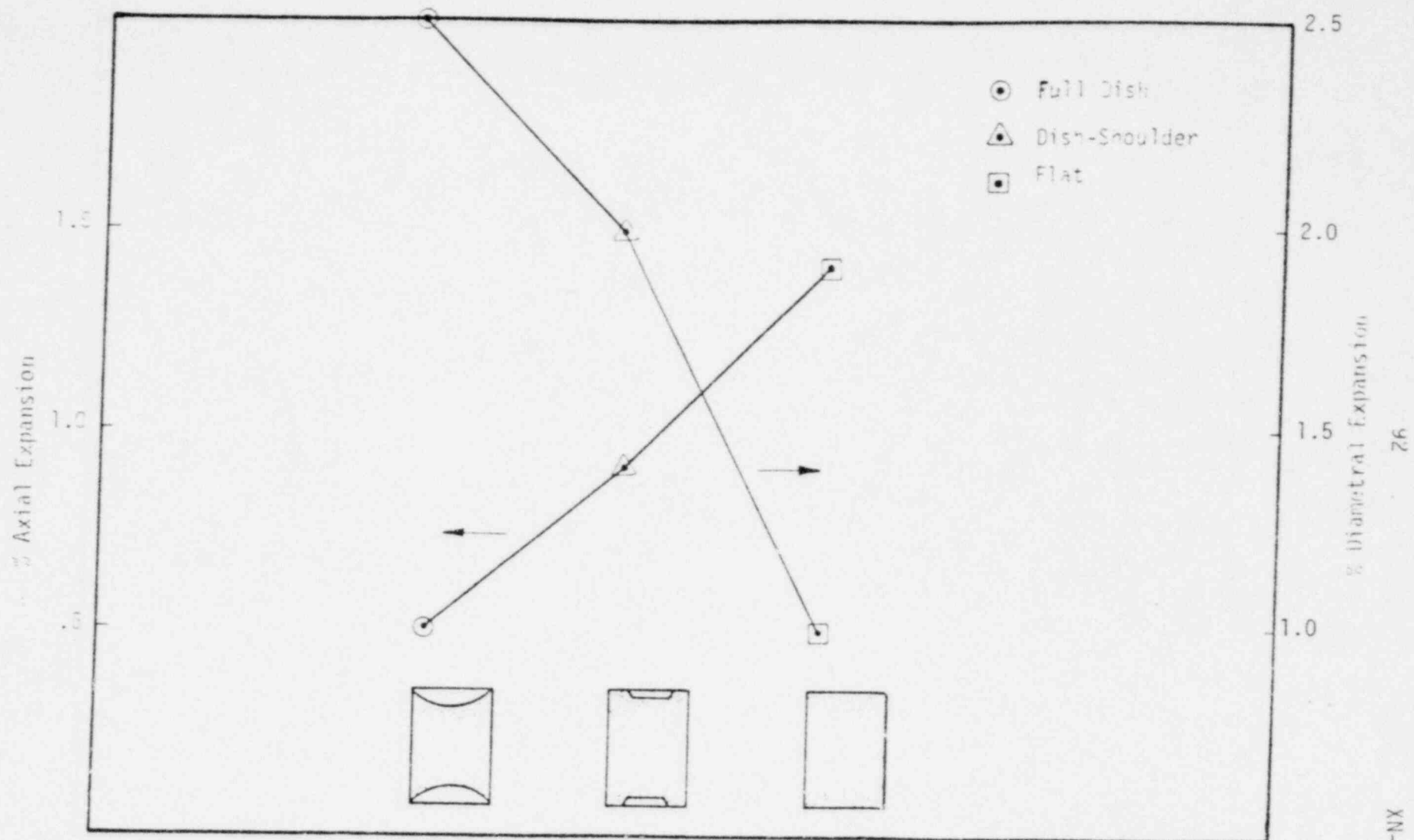


FIGURE 5-2

EFFECT OF PELLET GEOMETRY ON AXIAL AND
DIAMETRAL EXPANSIONS

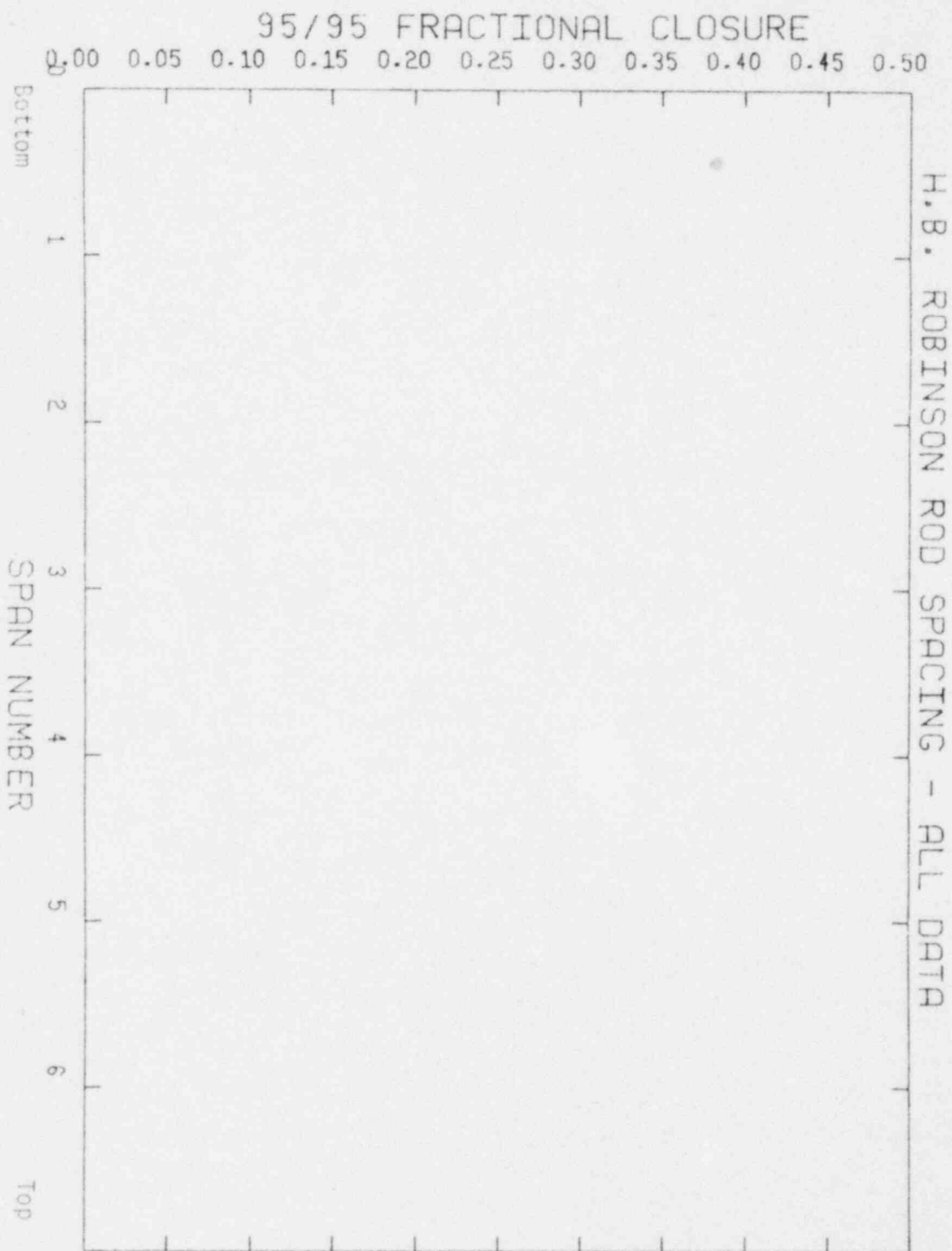


FIGURE 5.3 COMPARISON OF ROD-TO-ROD SPACING FOR ALL DATA

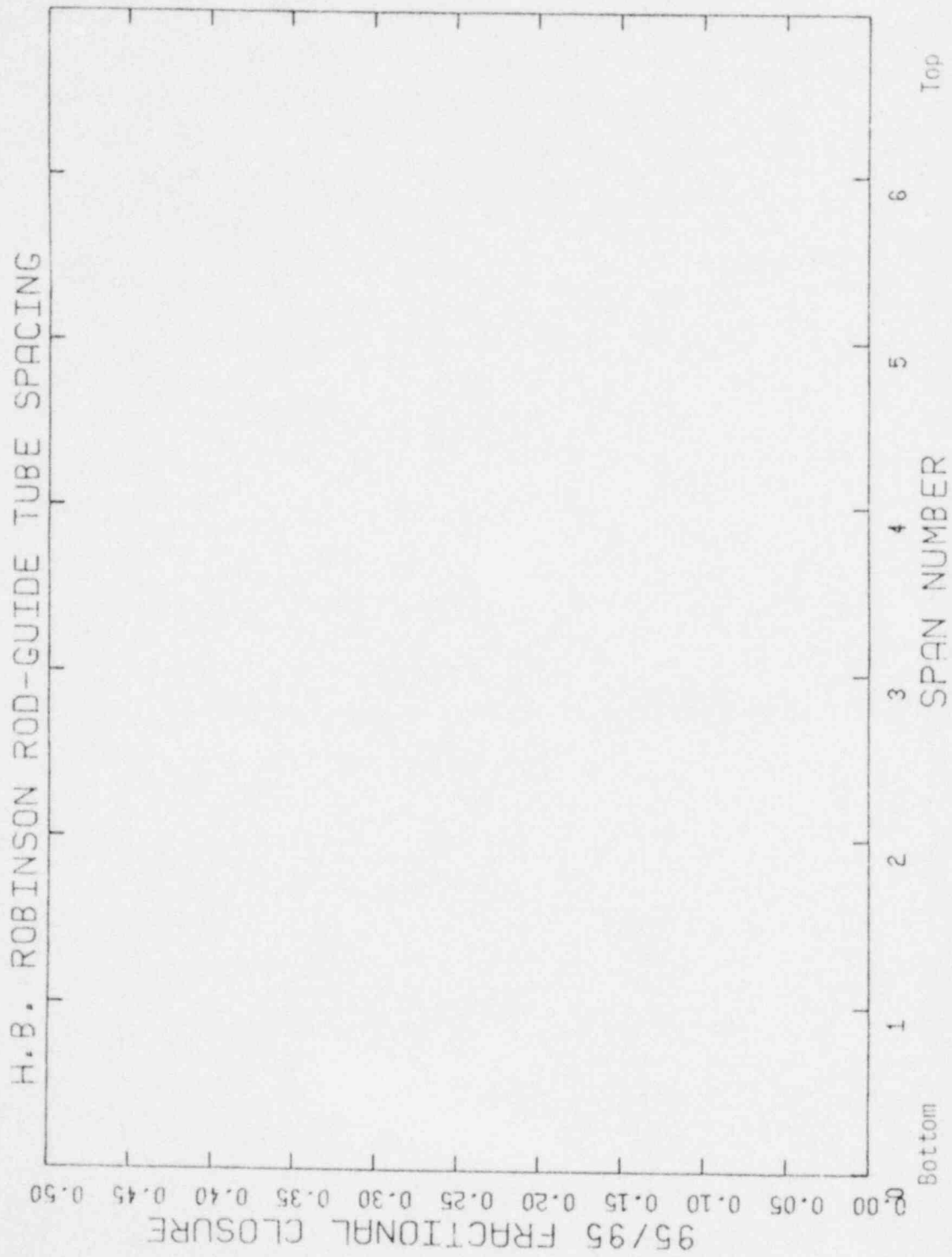


FIGURE 5.4 COMPARISON OF ROD-TO-GUIDE TUBE SPACING FOR ALL DATA

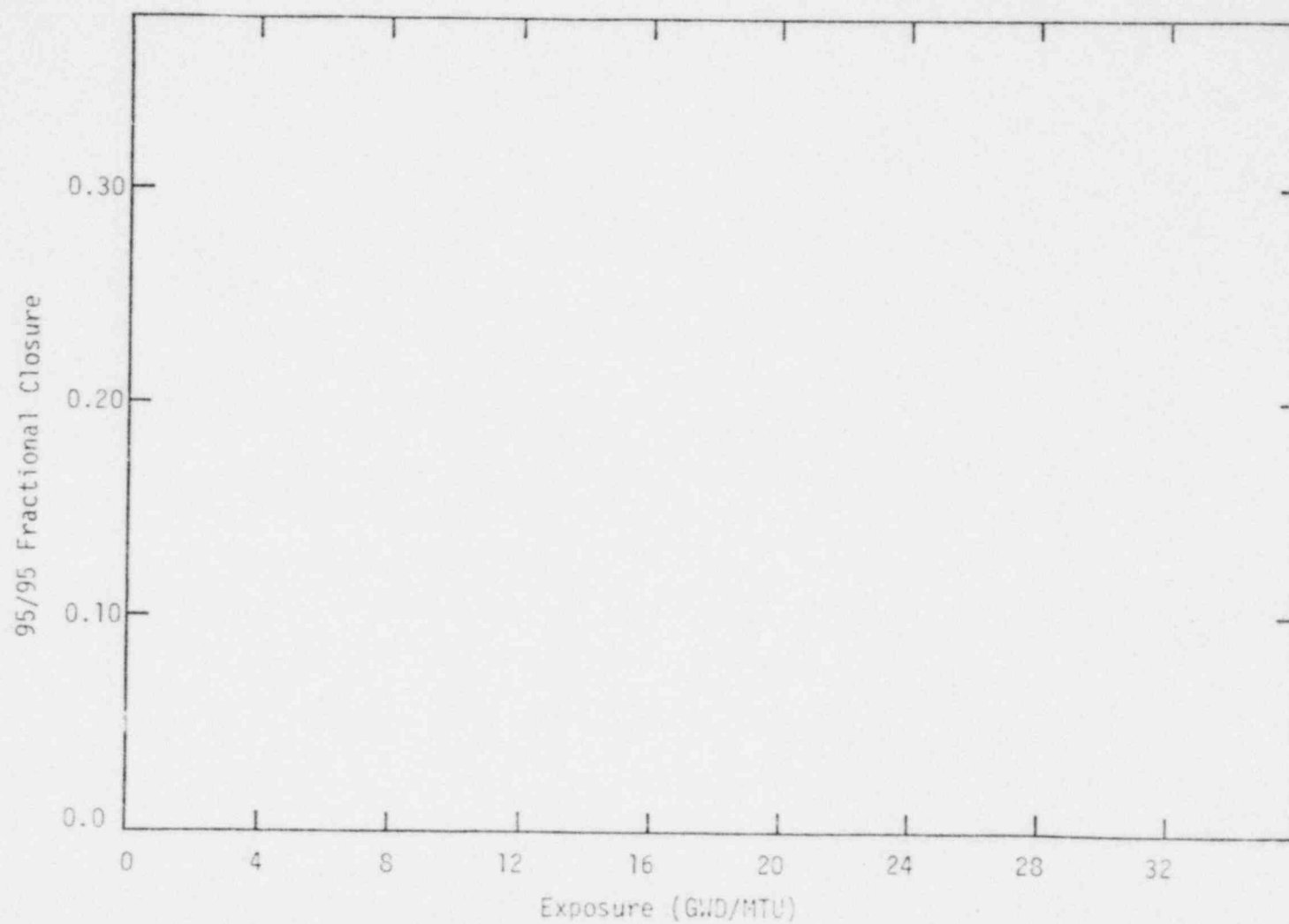
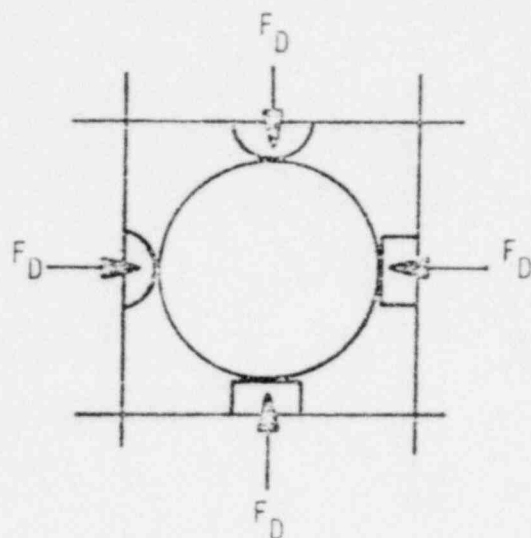


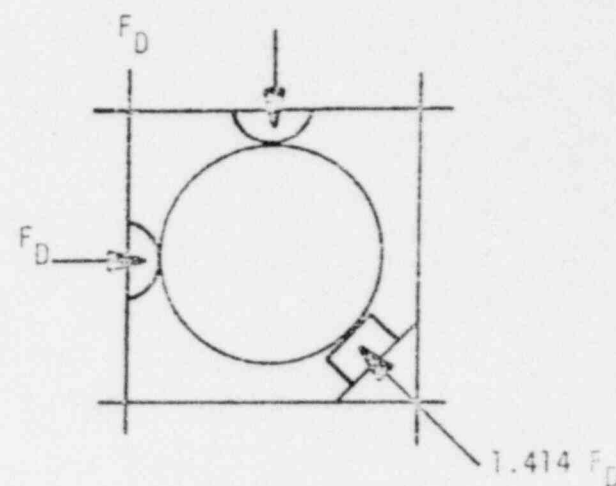
FIGURE 5.5 FRACTIONAL CHANNEL CLOSURE AT SPAN AS A FUNCTION OF ASSEMBLY AVERAGE EXPOSURE.

6 POINT FUEL ROD
SUPPORT



AXIAL FRICTION LOAD = $4.0 F_D f$

5 POINT FUEL ROD
SUPPORT



AXIAL FRICTION LOAD = $3.414 F_D f$

NET RESULT - 15% REDUCTION IN LOAD

FIGURE 5-6 AFFECT OF SPACER CELL GEOMETRY
ON AXIAL RESTRAINT

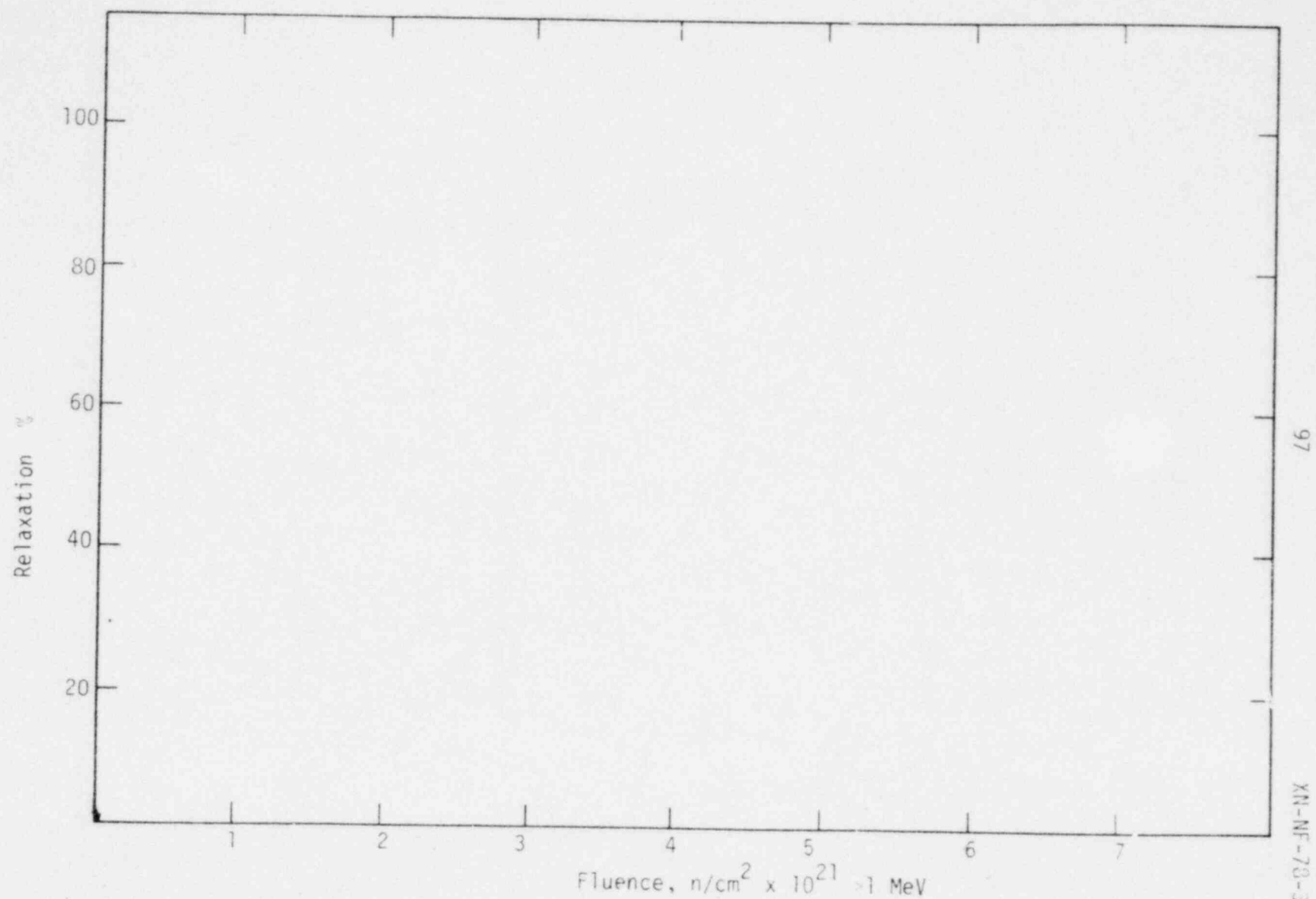


FIGURE 5-7

INCONEL 718 ESTIMATED SPRING
RELAXATION WITH IRRADIATION

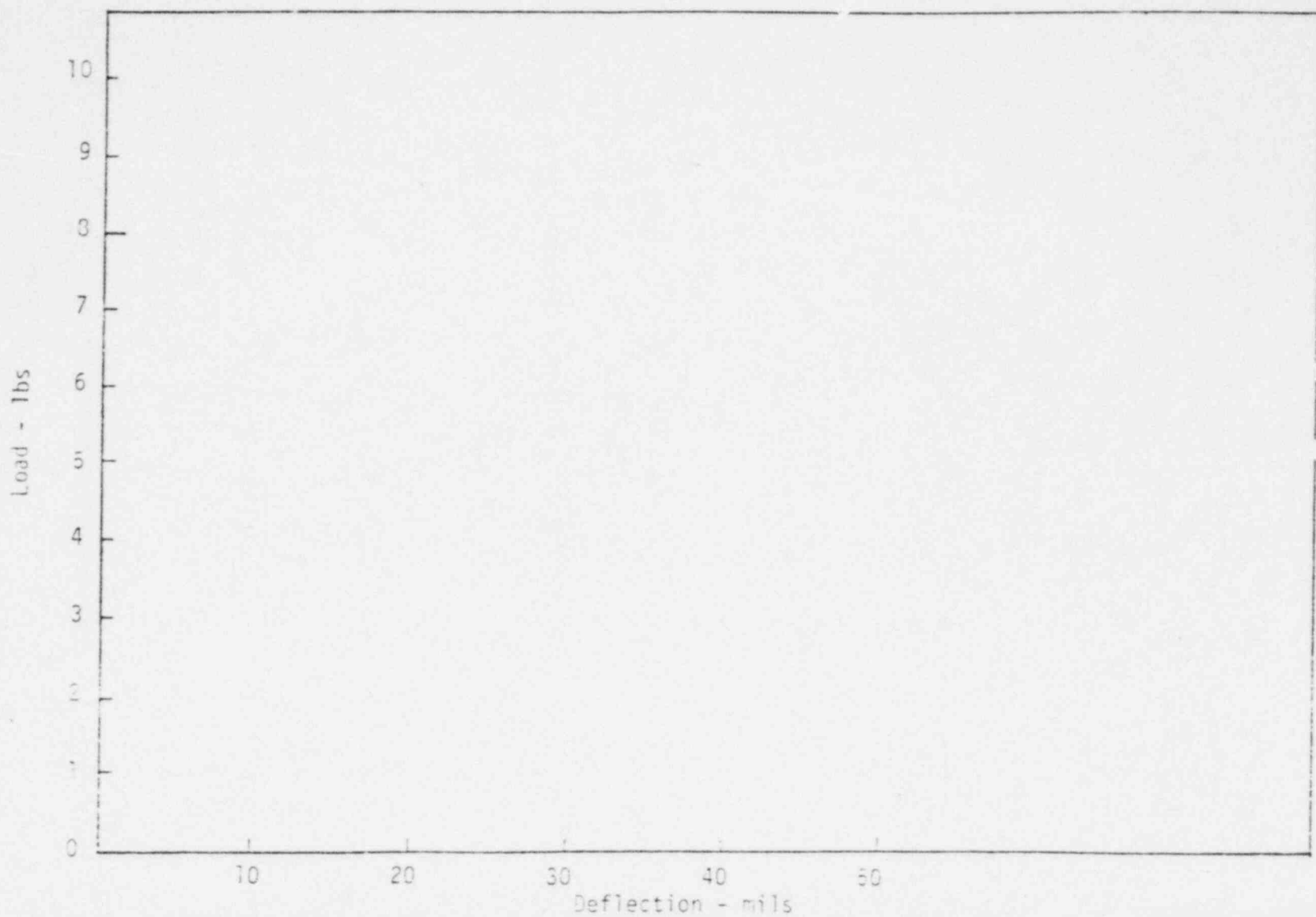


FIGURE 5-8 SPACER SPRING DEFLECTION VS. LOAD CURVES

FIGURE 5-9 ILLUSTRATION OF FLOW INDUCED VIBRATION OF A
FUEL ROD

FIGURE 5-10 ILLUSTRATION OF FORCES AND DEFLECTIONS
OF BOWED FUEL ROD

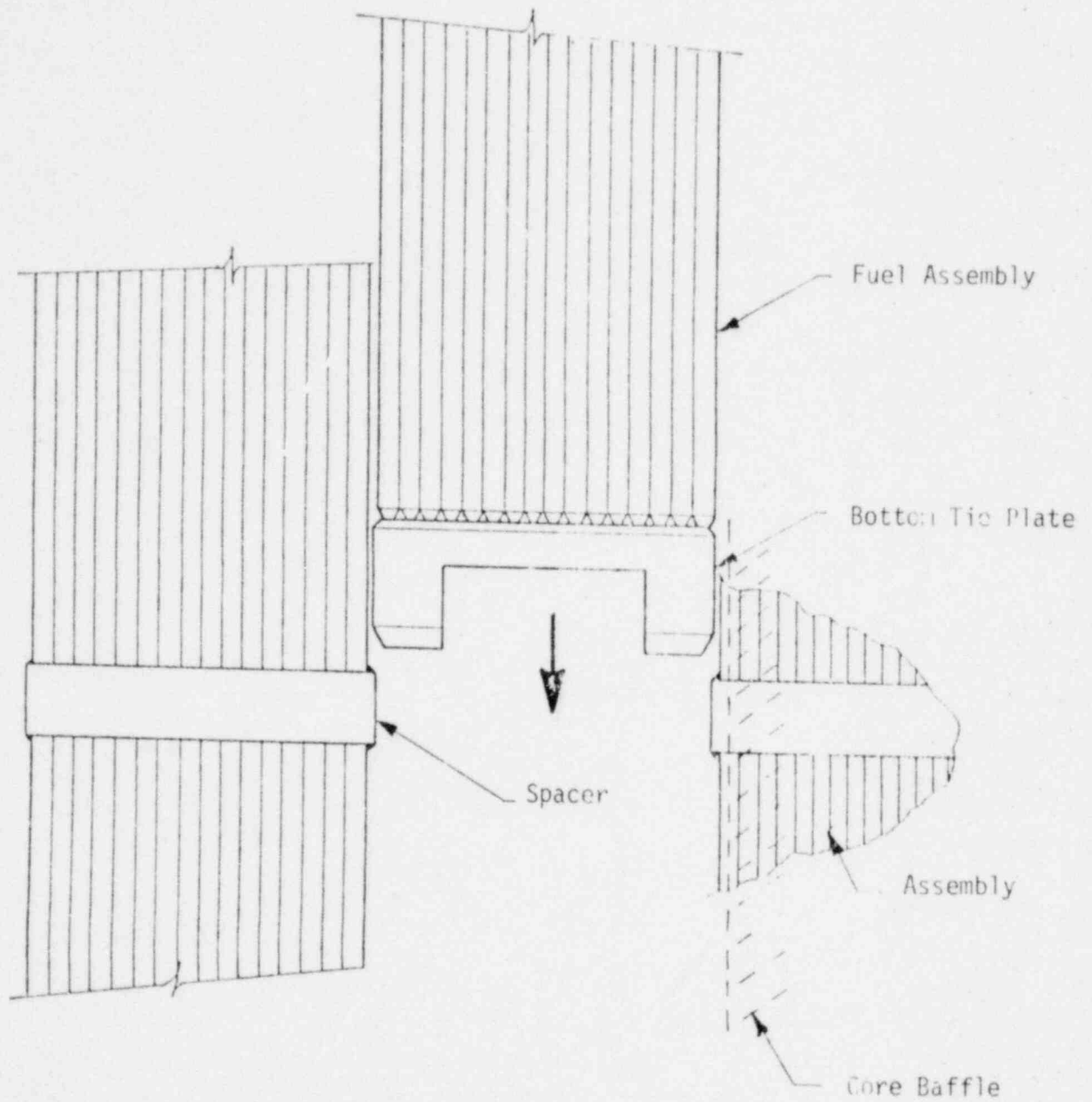


FIGURE 5-11

SCHEMATIC DIAGRAM OF FUEL BUNDLE STRIKING
THE TOP OF A SPACER GRID DURING BUNDLE
INSERTION INTO CORE.

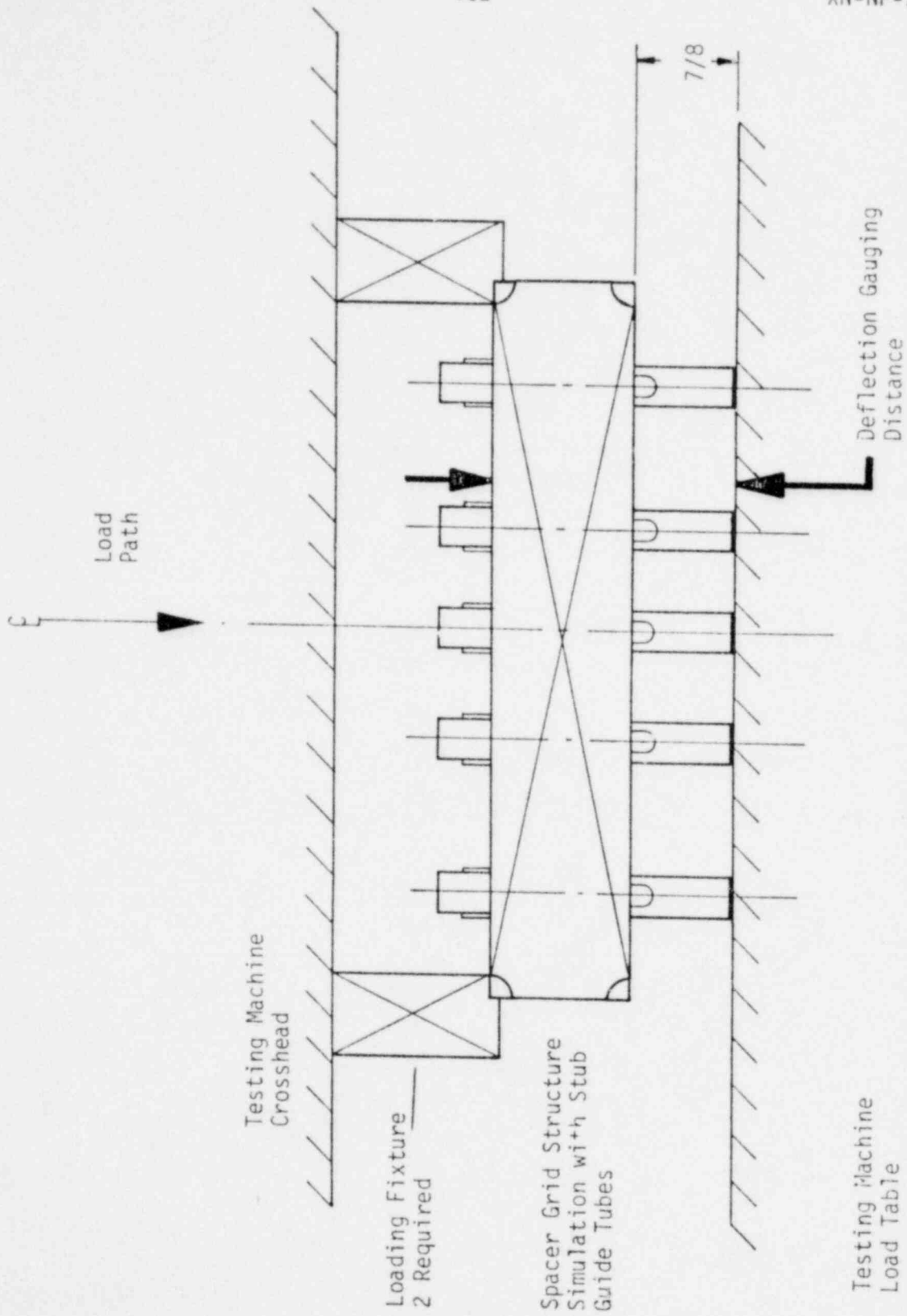


FIGURE 5-12 TEST ARRANGEMENT

6.0 FUEL TEMPERATURE ANALYSIS

Fuel temperature for the ENC fuel design are well below the UO_2 incipient fuel melting temperature of $2804 \pm 11^\circ\text{C}$ reported by Hausner⁽⁶⁷⁾. The fuel temperature calculations considered the effects of radial neutron flux densification, and pellet cracking in full conformance of the U. S. Nuclear Regulatory Commission approved ENC densification model.^(68,69)

, thermal conductivity data were the basis for the UO_2 fuel temperature calculation. The empirical fit of the data is:

$$K(T) =$$

where:

Integration of the algebraic thermal conductivity expression between zero and 2800 degrees Celsius yields This value is recognized to be somewhat less than that derived from other data, namely Robertson⁽⁷²⁾ which yields an integrated value of 97 watts/cm.

Corrections for the other densities, such as for in-reactor densified fuel, where with a Loeb type expression:

The film coefficient for predicting the cladding wall temperature was based on the Dittus-Boelter correlation for forced convection heat transfer and the Jens-Lottes⁽⁷³⁾ correlation for heat transfer during subcooled nucleate boiling.

Fuel densification and the corresponding changes in fuel density and pellet radius were calculated from the following empirical expression:

$$\begin{aligned}\Delta\rho/\Delta\rho_{\max.} &= [0.007 \ t] & t < 20 \\ \Delta\rho/\Delta\rho_{\max.} &= [0.2198 \ln(t) - .5184] & 20 < t < 1000 \\ \Delta\rho/\Delta\rho_{\max.} &= 1.0 & t > 1000\end{aligned}$$

where:

t = effective full power hours

$\Delta\rho_{\max.}$ = maximum fuel density after densification

and:

$$\Delta r = [\Delta \rho + 2\sigma] [r/3]$$

where:

σ = standard deviation in the measured probability distribution for pellet density

r = nominal as-fabricated pellet radius

The densification rate expressions were developed from the experimental data of Hanevik, et al.⁽²²⁾

The gap closure model, which results from pellet cracking and resultant pellet fragment relocation, was based on a detailed investigation of approximately 80 irradiated fuel pellet cross sections which showed that substantial closure of the initial pellet-to-cladding gap occurs at 600 hours of operation or after the first two or three power cycles.⁽²⁵⁾ Figure 3.8 illustrates the gap closure data. The data presented in Figure 3.8 were obtained from nine reactors and cover a broad range of physical parameters, i.e.:

- Density - 84 - 98% theoretical density
- initial gap size - 0.02 to 0.33 mm
- linear heat generation rate - 3 to 21 kW/ft

For the Exxon Nuclear Company fuel assemblies, the maximum fuel temperature conditions exist at beginning-of-life when the pellet-to-cladding clearance is maximum. This analysis determined the temperature profile across the fuel rod for the coincidence of several adverse conditions:

- 1) design overpower to account for transient operation
- 2) simultaneous power peaking at the same location using design peaking values
- 3) assume worst tolerances that maximize the cladding-to-pellet gap.

7.0 REFERENCES

EDITED

13. K. R. Merckx, RODEX: Fuel Rod Design Evaluation Code, XN-76-8, March 1976.
- 14.
- 15.
- 16.
- 17.
- 18.
19. D. Geithoff, et al., Irradiation Performance of Fast Reactor Fuels, International Symposium on Plutonium Fuels Technology, Proceedings of the 1967 Nuclear Metallurgy Composium held in Scottsdale, Arizona, October 4-6, 1967.
20. Technical Report on Densification of Light-Water Reactor Fuels, Regulatory Staff, U.S. AEC, November 14, 1972.
21. Additional Testimony on Point Beach-2 Nuclear Plant in Regard to Fuel Densification and its Effects, Prepared by Directorate of Licensing U.S. AEC, February 2, 1973.
22. A. Hanevik, et al., In-Reactor Measurements of Fuel Stack Shortening, presented at BNEW Conference (1973).
23. W. J. Kingery, Journal American Ceramic Society, 38, page 3 (1955).
24. J. A. L. Robertson, Irradiation Effects in Nuclear Fuels, an AEC Monograph, Gordon and Breach Science Publishers, New York, N.Y. 1969, page 309.
25. K. P. Galbraith, Pellet-to-Clad Gap Closure From Pellet Cracking, XN-73-17, June 1, 1973.

26. Deleted.
27. S. Kass, The Development of Zircalloys, ASTM STP-386, American Society for Testing Materials, 1961 Race Street, Philadelphia, Pa. 19103 (1964).
28. T. J. Pashos, H. E. Williamson, and R. N. Duncan, "Fuel Performance in Boiling-Water Reactors", Nuclear Applications, 3, December 1966.
29. A. B. Johnson, Jr., Effects of Nuclear Radiation on the Corrosion Hydriding, and Oxide Properties of Six Zirconium Alloys, ASTM-STP-458, November 1968. American Society for Testing Materials, 1961 Race Street, Philadelphia, PA 19103.
30. S. Y. Ogawa and M. F. Lyons, Power Reactor High Performance UO₂ Program, Final Progress Report No. 10, April-June 1969, GEAP-10042, June 1969.
31. K. Videm, Properties of Zirconium Base Cladding Materials, Corrosion and Hydrogen Pickup. Unpublished paper prepared for presentation at the "Advanced Course on Limiting Aspects of Fuel Element Performance in Water-Cooled Power Reactors", organized by the Netherlands, Norwegian Reactor School at Institutt for Atomenergi, Norway, August 24-28, 1970.
- 32.
33. Deleted.
34. Deleted.
35. Deleted.
36. H. Mogard, S. Aas, and S. Junkrans, Power Increases and Fuel Deflection, presented Fourth United Nations International Conference on the Peaceful Uses of Atomic Energy, Geneva, Switzerland, September 1971.
37. Deleted.
- 38.
39. ASME Boiler and Pressure Vessel Code, Section III, 1971 Edition, ASME, New York, NY.
40. W. J. ODonnell and B. F. Langer, "Fatigue Design Bases for Zircaloy Components", Nuclear Science and Engineering, Volume 20, January 1964.

41. M. P. Paidoussis and F. L. Sharp, "An Experimental Study of the Vibration of Flexible Cylinders Induced by Nominally Axial Flow", Transactions of American Nuclear Society, 11 (1), pages 352-353, (1968).
42. M. P. Paidoussis, The Amplitude of Fluid Induced Vibrations of Cylinders in Axial Flow, AECL-2225, March 1965.
43. H. S. Rosenbaum, "The Interaction of Iodine with Zr-2", Electrochemical Technology, Volume 4, Number 3-4, (March-April 1966).
44. A. Garlick, Stress Corrosion Cracking of Zirconium Alloys in Iodine Vapour, British Energy Conference, London, July 1971.
45. P. Sharifi and E. P. Popov, Refined Finite Element Analysis of Elastic Plastic Thin Shells of Revolution, December 1969.
46. S. Timoshenko, Strength of Materials, Part 2, D. Van Nostran, New York, NY, Third Edition, 1956.
47. J. F. Goodier, "Thermal Stress", Journal of Applied Mechanics.
48. S. Timoshenki and J. M. Gere, Theory of Elastic Stability, McGraw-Hill, New York, 1961.
49. R. J. Roark, Formulas for Stress and Strain, McGraw-Hill, Inc.
- 50.
51. B. A. Crea, R. R. Lewis, P. J. Pankiskie, JTEMP Computer Code, A Finite Element Heat Transfer Code, BNW-JN-75, December 1971.
52. B. A. Crea, P. J. Pankaskie, JSTRES - A Finite Element Stress Analysis Code, XN-CC-20, December 1971.
53. K. R. Merckx, Cladding Collapse Calculational Procedure, JN-72-23, November 1972.
54. To be published.
- 55.
- 56.

- 57.
- 58.
- 59.
60. M. J. F. Notley, A. S. Bain, and J. A. L. Robertson, The Longitudinal and Diametral Expansions of UO_2 Fuel Elements, AECL-2143, 1964.
61. K. R. Merckx, Computational Procedure for Evaluating Fuel Rod Bowing (AXIBOW), XN-CC-31, April 1975.
62. DTA 231, Revision 0, Design Test Authorization - R. E. Ginna Spacer Structural Tests, D. J. Cook, February 6, 1978.
63. STRESS-II User's Guide, UCC Computer Utility Network, UCC-102-3.
64. PTA-89, Revision 0 and PTA-132, Revision 1, Test Authorization for Bi-Metallic PWR Grid Spacer Development, dated October 9, 1973, and November 11, 1974, respectively.
65. W. C. Gallagher, PWR Upper Tie Plate Locking Mechanism Tensile Test for Flared Guide Tubes, XN-75-10, Revision 1, March 1975.
66. Deleted.
67. H. Hauser, "Determination of Melting Point of Uranium Dioxide", Journal of Nuclear Materials, 15, (3), pages 179-183, 1965.
68. "Technical Report on Densification of Exxon Nuclear PWR Fuels", USNRC, February 27, 1975.
69. K. P. Galbraith, "GAPEX: A Computer Program for Predicting Pellet-to-Cladding Heat Transfer Coefficients", XN-73-25, June 1975.
- 70.
- 71.

72. J. A. L. Robertson, et al., "Temperature Distribution in UO_2 Fuel Elements", Journal of Nuclear Materials, 7 (3) 225, 1962.
73. W. H. Jens and P. A. Lottes, "Analysis of Heat Transfer.